Student thesis series INES nr xx

Evaluation of High-Resolution Satellite Precipitation Products with Ground-Based Measurements over Europe

Svea Bertolatus

2020

Department of

Physical Geography and Ecosystem Science

Lund University

Sölvegatan 12

Svea Bertolatus (2020).

Evaluation of High- Resolution Satellite Precipitation Products with Ground -Based Measurements over Europe

Värdering av högupplösta satellitutfällningsprodukter med markbaserade mätningar över Europa

Bachelor degree thesis, 15 credits in *Physical Geography and Ecosystem Science*

Department of Physical Geography and Ecosystem Science, Lund University

Level: Bachelor of Science (BSc)

Course duration: *March* 2020 until *June* 2020

Evaluation of High- Resolution Satellite Precipitation Products with Ground -Based Measurements over Europe

---

Svea Bertolatus

Bachelor thesis, 30 credits, in *Physical Geography and Ecosystem Science*

Jing Tang

Lund University

Hossein Hashemi

Lund University

Exam committee:

Janne Rinne, Lund University

Abdulghani Hasan, Lund University

Abstract

Determining water quantity of precipitation, spatially and temporally is fundamental for weather forecasting, applications in hydrology and meteorology, climate science and for agriculture and industry. Only satellite measurements from space are able to perform large-scale measurements covering both, ocean and land. In order to prove the reliability of the satellite data for application, but also to develop and improve the satellite retrievals of precipitation data, the satellite products need to be evaluated with reliable ground-based measurements. The high-resolution satellite data that this study is based on, was provided at a global scale by the satellite network **G**lobal **P**recipitation **M**easurement (GPM) that builds an international constellation of research and operational satellites. Previous evaluation of GPM dataset have shown error characteristics, related to topography, climate and latitude, that are potentially linking back to the sensor input, such as the calibrated passive microwave estimates (PMW), being a fundamental source for the final product. Evaluating the PMW estimates over a large region can improve the understanding of the error sources in the combined final GPM product.

This study evaluated the calibrated PMW estimates (the primary foundation of the GPM IMERG final product) over Europe for the period from March 2014 to the end of December 2019 by using the blended gauge data from, provided by European Climate Assessment and Dataset (ECA&D), as reference. The data was evaluated seasonally, conducting different error indices to compare the satellite product with the gauge data and linking it to topography, climate and latitude.
The results showed clear relationships between PMW data accuracy with elevation and climate zones in Europe, that can be linked to difficulties for PMW sensors to measure e.g. frozen precipitation, observe from a cold background, or when convection occurs in warmer climates. Also, for the relation to latitude, a worse performance with latitude was found, however only in winter, when frozen precipitation is likely at higher latitudes.
Correcting those input sources, based on accuracy assessments, such as it was assessed by this study, can be meaningful for further improving GPM product.

Keywords: *Precipitation, satellite product evaluation, passive microwave, estimates, Europe, ground-based gauge data*

Acknowledgements

I would like to acknowledge my supervisors and experts Jing Tang and Hossein Hashemi, who have both giving me impressive support. Therefore, I want to thank Jing, especially for her guidance and help in coding, and knowing the “how to”, whenever I was stuck. And I want to thank Hossein for his experience and knowledge in the topic, giving me guidance and motivation for the study and it`s improvement.
I also want to thank the Department of Physical Geography for providing a great Bachelor program and study atmosphere. It has been very happy three years, not least because of my lovely classmates.

Furthermore, I want to thank my family. Without my family´s support, even in distance, I would not be where I am now, and not as happy either. Miss you.
Thank you, also to my friends whether in Sweden, Germany or very far away. A special thanks to Pamela, Tanja, Yi Wen and Serena - for their support, energy, and laughter, from Sunday brunches to midnight studies. And lastly, thank you, Johan, for the encouragement and happiness that you are giving me.

Contents

1. Introduction

Climate is warming at global scale and climate models have predicted both, an increase in temperature, but also a change in precipitation pattern in the near future. Precipitation is the water that is formed in the atmosphere and reaches to the Earth in liquid or frozen forms and is of high importance to establish and maintain life on Earth. Precipitation varies largely at both, spatial and temporal scale (Geographic 1996). How precipitation will change in response to future climate change is unclear and climate models often have large uncertainty range for predicting precipitation changes (Nazemi et al. 2014).

Energy is released when water vapors condense into liquid precipitation (NASA 2014). This part of energy (latent heat) that is released into the atmosphere, can be taken as an estimate of the amount of precipitation formed. Latent heat is one of the important driver of atmospheric circulation, together with solar radiation. That implies that knowledge about precipitation amount and distribution are of importance for climate research (NASA 2014).

Furthermore, increased or decreased precipitation can have effects on ecosystems and society. It is certain that a change in precipitation will influence the runoff pattern and redistribution of water in space, resulting in flooding or drought in different places, bringing challenges for the society (Alliance 2018). Hence, determining water quantity of precipitation spatially and temporally is fundamental for weather forecasting, applications in hydrology and meteorology, climate science and for agriculture and industry (Silva Lelis, 2018 Lee et al. 2019).

Precipitation measurements are provided as depth of water, to what depth it would accumulate on the earth surface per unit time (e.g. mm/day). At the moment, there are three different methods to measure precipitation: ground networks of rain gauges, ground-based weather radars, and satellite measurements by satellite-based radiometers (Kucera et al. 2012).

The easiest method is to conduct in-situ measurements by rain gauges, giving point measurements on the earth surface (Brandt et al. 2017). Those ground-based measurements allow relatively accurate precipitation measurements at the location of the climate station. However, gauges are expected to underestimate snow accumulation, and might also show undercatch due to winds, trace precipitation or wetting losses (Zhang et al. 2019).

The remaining two methods, weather radars and satellite measurements, are operated by meteorological organizations (Brandt et al. 2017). Ground based weather radars are able to display the distribution and measure the amount of precipitation over a local area, on a plan position indicator using echo power (Harrold 1966).

Only satellite measurements from space are able to perform large-scale measurements covering both, ocean and land. Global satellite measurements of precipitation are based on only microwaves, microwaves that are calibrated with infrared (IR) observations or a combination of microwave and infrared observations (Hou et al. 2013). Nowadays satellites can even have a Dual Frequency Precipitation Radar (DPR) on board, as e.g. the Global Precipitation Measurement Mission (GPM) core satellite does. Despite IR sensors infer precipitation estimates from brightness temperature at the top of clouds to estimate precipitation (Gebregiorgis et al. 2018), microwave sensors are performing better as they capture microwave radiance that is emitted from precipitation droplets, liquid in low frequency and iced in high frequency channels (Hou et al. 2013; Gebregiorgis et al.

2018), as the droplets influence the natural occurring electromagnetic emissions of the earth (Gebregiorgis et al. 2018). It is noted that the passive microwave (PMW) sensors are less accurate in terms of temporal resolution, as they fly on low earth orbit satellites, revisit a site less frequent due to the low orbitography of the satellite. In order to receive the highest accuracy and best temporal and spatial resolution, IR and PMW information need to be combined (Gebregiorgis et al. 2018).
There are areas that have a high density of those gauge or radar stations, for example northern and central Europe (Singh et al. 2015). However, in other parts, such as oceans, parts of developing countries, complex mountainous terrain, that cannot be easily accessed, and areas with a lower population, ground measurement stations are sparsely distributed (Xu et al. 2017; Sunilkumar et al. 2019). Therefore, high resolution satellite data can be used as a complement for these areas (Khodadoust Siuki et al. 2017). In order to prove the reliability of the satellite data for application, but also to develop and improve the satellite retrievals of precipitation data, the satellite products need to be evaluated with reliable ground-based measurements (Lee et al. 2019).

The high resolution PMW satellite data in liquid and ice state that this study is based on, was provided at a global scale by the satellite network **G**lobal **P**recipitation **M**easurement GPM that builds an international constellation of research and operational satellites (NASA 2014). More information on these satellite data is provided in section 3.1.1.
By providing more accurate precipitation data covering a large area, GPM is expected to improve knowledge about water cycle and how precipitation processes respond to climate change. Furthermore, it is also a requisite for improved water resources management, as products provide information about freshwater resources. This level of information is also important for the development of mitigation strategies to optimize practices for the optimal use of water resources (Sunilkumar et al. 2019; Maghsood et al. 2020).
In addition, GPM products are also likely to give an insight on clouds and aerosol activity as they are able to observe clouds and particles. That is why GPM is expected to give information about how human activities influence precipitation processes (NASA 2014).

Integrated **M**ulti- satellit**e**s **R**etrievals of **G**PM (IMERG) combine the information of PMW and IR platforms into half hourly gridded fields. Validations for the GPM IMERG products have been done for, e.g., the southern Tibetan Plateau (Xu et al. 2017), Iran (Maghsood et al. 2020), south-eastern Austria (Sunilkumar et al. 2019), United States (Gebregiorgis et al. 2018). For Europe, the GPM IMERG final product has been evaluated by a very recent study, based on the gridded dataset "ENSEMBLES OBServation" (Navarro et al. 2019), focusing on the accuracy of the GPM data over mountainous areas. In general, earlier studies have shown that satellite measurements tend to underestimate precipitation in the high elevation areas (Hirpa et al. 2009; Hashemi et al. 2017; Maghsood et al. 2020). Furthermore, it is likely that satellites, but also weather radars, underestimate snowfall accumulation, because snow is generally difficult to measure by satellite sensors (Wen et al. 2016).
Thus, underestimation is generally expected to occur in high altitudes but also with higher latitudes in Northern Europe, where snowfall is a common form of precipitation in the wintertime. As mentioned, also gauges are recognized to undercatch, especially the light or frozen form of precipitation (Zhang et al. 2019). This might result in a double effect of underestimations at higher

elevation or higher latitude, in the evaluated but also the reference data, when gauge data is used as reference for satellite evaluation.
Despite that, a study also showed that satellite performances are likely to be better in a cold climate, when the weather is determined by stratified systems and not convective storms that characterize a warm climate (Maggioni et al. 2017).

1.1 Study Aim

Previous evaluation of GPM dataset focusing on different regions and using different reference data sets have shown similar error characteristics, potentially linking back to the sensor input. It is known that the sensors of the GPM constellation perform differently due to the differences in "scan strategies, instrument channels, and footprint size" (Tan et al. 2020). The existing biases of each sensor are alleviated by the inter-calibration of the PMW information by different sensors. Evaluating the PMW estimates over large-region can improve the understanding of the error sources in the combined final product (Tang et al. 2014).

Therefore, this study aims to evaluate the reliability of calibrated PMW estimates (the primary foundation of the GPM IMERG final product) for the period from March 2014 to the end of December 2019 by using the blended gauge data, provided by European Climate Assessment and Dataset (ECA&D), as reference. The seasonal averages of satellite are evaluated, using different error indices to compare the satellite product with the gauge data. It is hypothesized that the accuracy dependence of the GPM Final Product on topography, latitude and climate can be seen already in the input source to the algorithm, the PMW estimates.
Hence, the secondary aim of this study is to link the accuracy of the satellite-based precipitation data with other geographical properties, such as topography, climate zones, and latitude.

2. Background of the study area

The study area for the GPM IMERG evaluation is Europe, one of the seven continents of the earth, located in the Northern Hemisphere. Geographical seen, it is the Western part of the Eurasian landmass but also including outstanding islands and countries, such as Iceland and Great Britain. Europe borders to Asia in the east, the Mediterranean Sea in the south, the Atlantic Ocean in the west and the Arctic Ocean in the north. The study focuses on Europe with an extend from 83°00' North to 30° 00´South, and 30°00´ West to 70°00´ East.

As studies show, satellite performance is dependent on climate and topography (Hirpa et al. 2009; Hashemi et al. 2017; Maghsood et al. 2020, Wen et al. 2016, Maggioni et al. 2017). Thus, topography and the climate zones of Europe are introduced in bellows sections.

2.1 Topography

Europe is characterized by a few mountain chains and elevated areas. Figure 1 shows the digital elevation model (DEM) GTOPO30 over Europe (CBI 2010). For a better insight on the topography over Europe, the continent can be grouped into four different regions, which are the Western Uplands, the North European Plain, the Alpine Mountains and the Central Uplands (Geographic 1996).

Effects of glaciation caused mountainous landscapes throughout Scandinavia, mostly covering Norway. Scandinavia, together with Iceland, Scotland, Ireland, Brittany (France), Spain and Portugal build the group of Western Uplands (Geographic 1996).
The North European Plain stretches from England over Northern France, Belgium, the Netherlands, Germany, Poland, Denmark, Estonia, Latvia and Lithuania to Russia, and is characterized by a very low area (Geographic 1996).
Further to the South of Europe, the Alpine Mountains, combine the mountain chains Alps (covering parts of France, Swiss, Austria, and southern Germany), the Pyrenees, being the natural border between France and Spain, the Apennine Mountains in Italy, Dinaric Alps in Southeastern Europe, the Balkan Mountains in East Balkan, and the Carpathians, ranging through Central and Eastern Europe (Geographic 1996).
Furthermore, the Central Uplands are stretching in Central Europe from west east, covering France and Belgium, southern Germany, northern Switzerland, Austria, and the Czech Republic. The area is characterized by forests and low-density population (Geographic 1996).

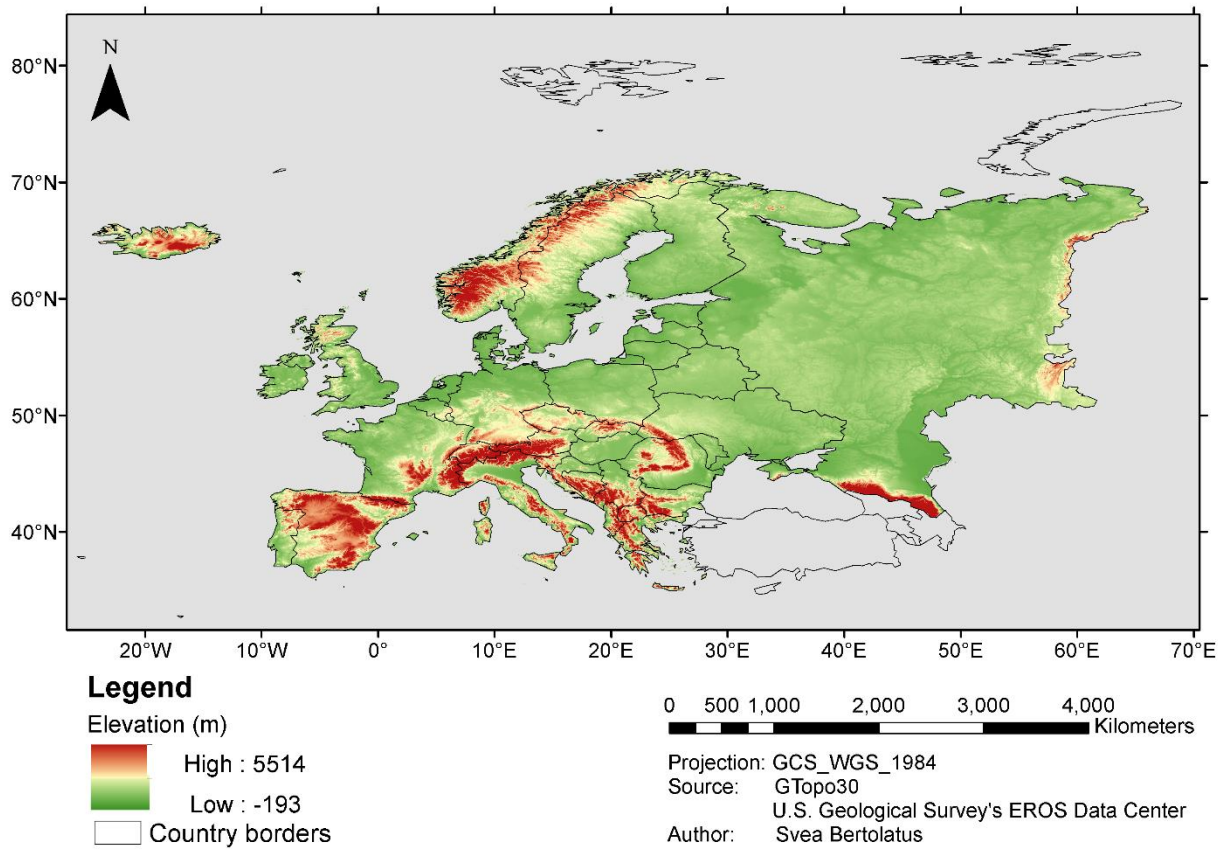

Figure 1: Digital Elevation Model (DEM) of Europe with country borders.

2.2 Climate

The large extent of Europe allows the climate to vary. According to the Köppen/Geiger climate classification (1898), in Europe four main climate zones can be distinguished (Figure 2). The central and western Europe is characterized by a temperate oceanic climate (Cfb), meaning a mild temperature between 0 °C and 22 °C, whereby the summer is warm. Precipitation does not vary during the year and there is no dry period (Mindat 2000).

Eastern Europe is characterized by warm summer and humid continental climate (Dfb), that differs from Cfb as the temperature can go under 0 °C. Temperature also rises in summer, with an average of 22 °C. In this area, the precipitation also does not show significant changes between the seasons (Mindat 2000).

A boreal climate (Dfc) is present in the northern Europe, featured by cold temperatures, and even a cold summer. Temperature can fall below 0 °C in the cold season while the precipitation does not change significantly seasonally (Mindat 2000).

The arctic region in norther Europe, such as Iceland and parts of Scandinavia, experience Tundra (ET). Here, the average temperatures all year around lie between 0 and 22 °C. This can also be found at very high altitudes in the Alps, together with Dfb and Dfc (Figure 2).

The warmest climate is found in southern Europe. Here, the hot-summer Mediterranean climate (Csa) is most common. It is characterized by hot summers, and mild temperatures during the rest of the year, which do not fall under 0 °C. Precipitation amounts are higher in the winter than in the summer (Mindat 2000).
Figure 2 presents the climate zones and shows five station locations, of which precipitation data will be further analyzed, as it is described in section 3.1.4.

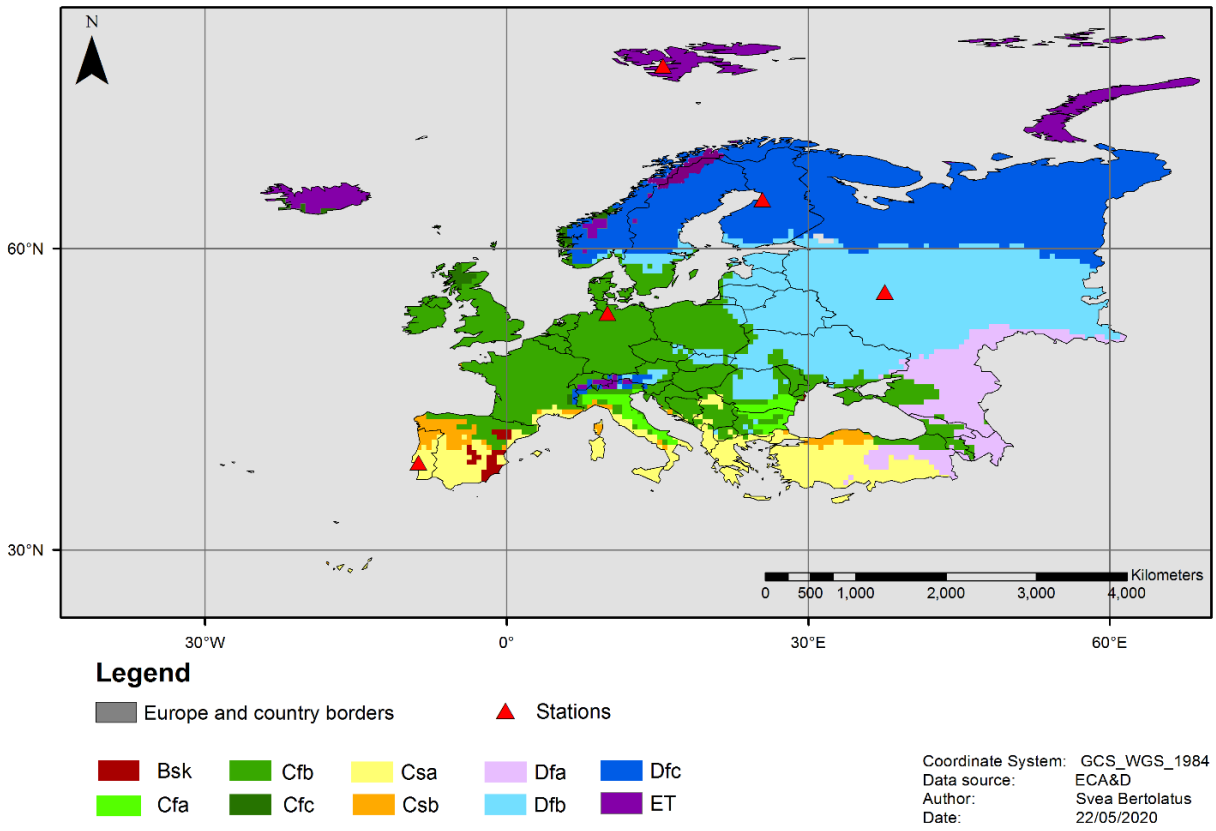

Figure 2: Köppen/Geiger climate classification of Europe (Source: (Bank 2017; Beck et al. 2018)): cold semi-arid climate (Bsk), humid subtropical climate (Cfa), temperate oceanic climate (Cfb), subpolar oceanic climate(Cfc), hot-summer Mediterranean (Csa), Warm-summer Mediterranean(Csb), humid continental climate(Dfa), humid continental climate (Dfb), boreal climate (Dfc), tundra climate(ET); and weather stations from North to South: Svalbard, Oulu, Moscow, Hamburg, Lisbon.

3. Methods

The section of Methods presents the description of data, and procedure (data preparation and data analysis) for each dataset.

3.1 Data description

The datasets used in this study are summarized in Table 1 and described in the following sections.

Table 1: Summary of datasets used in this study.

ID	Datasets	Source	Spatial extent	Format, Resolution
1	Satellite data	GPM IMERG V06, Final Product, PMW precipitation estimates	90° N to 90°S: partial coverage; 60° N and 60°S: full coverage	Gridded NetCDF Spatial: 0.1° Temporal: 30 min , summed to daily accumulation
2	Gauge data, ground-based	ECA Dataset, blended ground-based station measurements	Europe and Mediterranean area	ASCII Vector (Point) Temporal: daily
3	Digital Elevation Model	GTOPO30	Global	Raster Spatial: 30 arc seconds
4	Köppen climate classification	Beck, H.E. et al. 2018 The world bank (2017)	Global	Vector (Polygon)

3.1.1 Satellite data

The GPM mission was initiated in 2014 and thus, data are provided from March 2014. It is led by the Japan Aerospace Exploration Agency (JAXA) and National Aeronautics and Space Administration (NASA) and consists of several other international space agencies:

- Centre National d'Études Spatiales (CNES)
- Indian Space Research Organization (ISRO)
- National Oceanic and Atmospheric Administration (NOAA)
- European Organization for the Exploitation of Meteorological Satellites (EUMETSAT)

and others.

Provided is full coverage of the earth between 60° North and 60°South and "partial coverage" between 90° North and 90°South (NASA 2014) for every 30 minutes and a spatial resolution of 0.1 ° (Xu et al. 2017).

The GPM mission is the successor of the Tropical Rainfall Measuring Mission (TRMM) that was also initiated by NASA and JAXA. TRMM was launched in 1997 and ended on the 15th of April 2015, when the fuel was depleted. The TRMM mission provided precipitation measurements for 17 years in tropical and subtropical regions where about two thirds of the global rainfall occurs, covering the globe from 50° North to 50° South (NASA 2014). Measurements were done with the use of a precipitation radar (PR) to observe precipitation and storm pattern, and TRMM Microwave imager (TMI), to measure the emitted energy by earth and atmosphere in order to determine the amounts of water vapor, cloud water and the intensity of precipitation (NASA 2014). TRMM data are included in the GPM dataset from 2000.

GPM, just as TRMM, include both active and passive sensors to measure the precipitation properties. Active Radars, such as the GPM Dual Frequency Precipitation Radar, receive and transmit signals. The GPM mission is a constellation of partner satellites consists of a "core observatory'' satellite that carries a radiometer system for the precipitation measurements from space, and also acts as a standard reference for the research and operational satellites network. In this way it is possible to unify the measurements of PMW and IR satellite platforms. **I**ntegrated **M**ulti- satellit**e**s **R**etrievals of **G**PM (IMERG) combine the information of PMW and IR platforms into half hourly gridded fields.

GPM IMERG is the multi- satellite data product that is used for the understanding of precipitation distribution and variability. There are three different products for various user requirements, differing in latency and accuracy: Early (ca. 4 hr.), Late (ca. 12 hr.) and Final (3.5 month) products. While the early run can be used for analysis of flash floods and the late one for crop forecasting, the final one is produced for research, as it is already calibrated with gauge measurements to achieve a higher accuracy (NASA 2014).

Because the final product is already calibrated with gauge data, it performs better and is used for research purposes. Stations for used for calibration are, however, not the same as the reference gauge data used in this study and the latter dataset consisting of more stations.

In this study the PMW estimates are evaluated, being considered as the "backbone"(Tang et al. 2014) of the combined satellite product. The analyzed PMW estimates have a spatial resolution of 0.1° and are accumulated products are available for each day of the study period.

3.1.2 Ground based gauge data

The European Climate Assessment and Dataset project (ECA&D) provides data on climate extremes, but also daily climate measurements, over Europe and the Mediterranean region. Parts of the data are available on the project's website, without costs, for non- commercial use in science and education (Dataset 1998).

The project was initiated in 1998 by EUMETNET, which is a network of 31 European National Meteorological Services (Network). It is financially supported by EUMETNET as well as the European Commission. The project provides series of daily data for 19087 meteorological stations by 77 participants. The distribution of climate stations, presented in Figure 4, shows the densest

spread of stations in the middle Europe, Ireland and Scandinavia and a sparse spread in other parts of Europe and the Mediterranean region.
Besides the daily precipitation amount, measured by gauge stations, the ECA&D dataset include temperature (maximum, minimum, and mean), sunshine, snow depth, cloud cover, global radiation, wind, humidity, and sea level pressure. The available data are the *blended* (used in this study), and *non-blended* data series, whereas blended means that data from e.g. two nearby stations with an overlap in the time period, has been unified and merged, a process that can be done seamlessly (Dataset 2020). The *non- blended* data thereby provides the separate underlying data series of e.g. the two different stations (Dataset 2020). The source data has not undergone more changes, it was kept as it was received from the participants (Dataset 2020).
Precipitation data is provided for each station location accumulated observations for each day of the study period, in ASCII format, whereas coordinates for each station are found in a separate source file.

3.1.3 Digital Elevation Model (DEM)

The DEM GTOPO30 was downloaded from the website of ArcGIS, provided by the U.S. Geological Survey's Center for Earth Resources Observation and Science (EROS) and Conservation Biology Institute (CBI). GTOPO30 is a DEM of global coverage with a spatial resolution of 30-arc second (about one kilometer). The EROS data center updates and maintains the data since 1993. Topographic areas have been introduced for the reader to have elevated areas in mind and receive a picture of the topography of Europe.

3.1.4 Climate Classification

A polygon file of the Köppen climate classification, downloaded from World Bank (Bank 2017) was used as guidance for the area extent of the different classes. The climate class distribution was obtained from the study "Present and future Köppen-Geiger climate classification maps at 1-km resolution" (Beck et al. 2018) and combined with the world bank polygon file.

To analyze the dependence of PMW accuracy dependent on a climate zone, five locations across Europe were chosen, representing the largest climate zones in Europe, and picked to analyze the stated hypothesis with those five examples. Locations from North to South (Figure 2) were:

Table 3: Locations for further analysis and related climate zones.

Location Name	Climate zone
Svalbard, Norway	Et (Tundra)
Oulu, Finland	Dfc (boreal climate)
Hamburg, Germany	Cfb (temperate oceanic climate)
Moscow, Russia	Dfb (warm summer humid continental climate)
Lisbon, Portugal	Csa (hot-summer Mediterranean)

3.2 Data preparation

All datasets were adjusted in terms of study area, to the spatial resolution and format. Both, PMW data and gauge data was already available as daily precipitation accumulation, thus, no adjustments were made for the temporal resolution.

3.2.1 Satellite data

The satellite data were downloaded as NetCDF (.nc4) files from the data collections of Goddard Earth Sciences Data and Information Services Center (GES DISC) for each day in the time period from March 2014 to December 2019 covering the whole globe with 90° North and 90° South, longitude 180° West and 180° East with a spatial resolution of 0.1° (Huffman et al. 2019). In the geographic information system ArcMap 10.5 the NetCDF files were visualized by creating a raster layer. Further operations to the satellite data were carried out in the MATLAB R2019b environment. The satellite data files for each day in the study period were cropped to the extent of the study area. The Europe extend was given by a shapefile of Europe.

3.2.2 Ground based gauge data

The daily precipitation gauge data was available for 13,820 stations and downloaded as ASCII files, containing StationID, the date in format yyyymmdd, the precipitation amount, and a quality code. The files were trimmed to only include the appropriate time range from March 2014 to the end of 2019, and station coordinates were added to the files using MATLAB R2019b.

A lot of stations showed missing data from a couple of days to months. In order to include as many stations in the analysis as possible, the text files were grouped according to the percentage of available measurement that overlaps with the daily satellite measurements, during the study period (Figure 3), whereas, e. g. >10 % includes all stations, having 10-100 % of available data overlaps with the GPM data. The stations that were chosen for evaluating our satellite data have more than 80% of data overlay with our satellite data in this study (Figure 4). This group was chosen, because in the seasonal data analysis, the number of data points, temporally seen, can be assumed to be fairly equal throughout the four seasons. Furthermore, Figure 3 shows that about 2000 more stations could be included in the analysis, relative to only using the stations with 100% temporal overlaps with the GPM data. All of the ASCII files (of each gauge station) belonging to the group of >80 % overlap, were taken together in matrices, rearranged, and then converted to NetCDF, in order to have the same format as the PMW data.

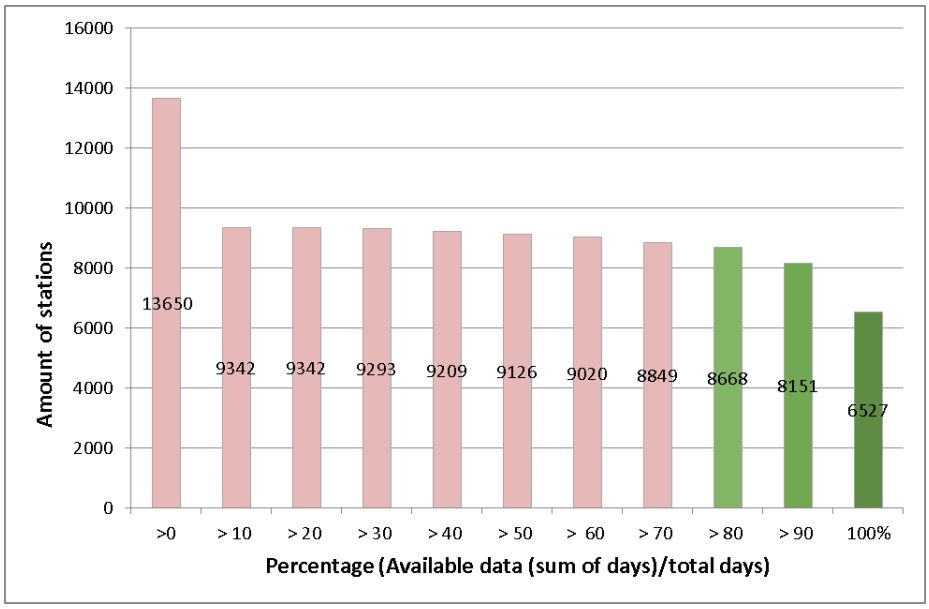

Figure 3: Number of stations with different temporal overlap with the GPM data, whereas, e.g., >20 represents percentages of 20 to 100% overlap. Rose colored bars represent data groups that could include data stations with more than 20% of missing data. Green colored bars show groups that had enough data to be fairly equal throughout all seasons, whereas the group >80% was used for further analysis.

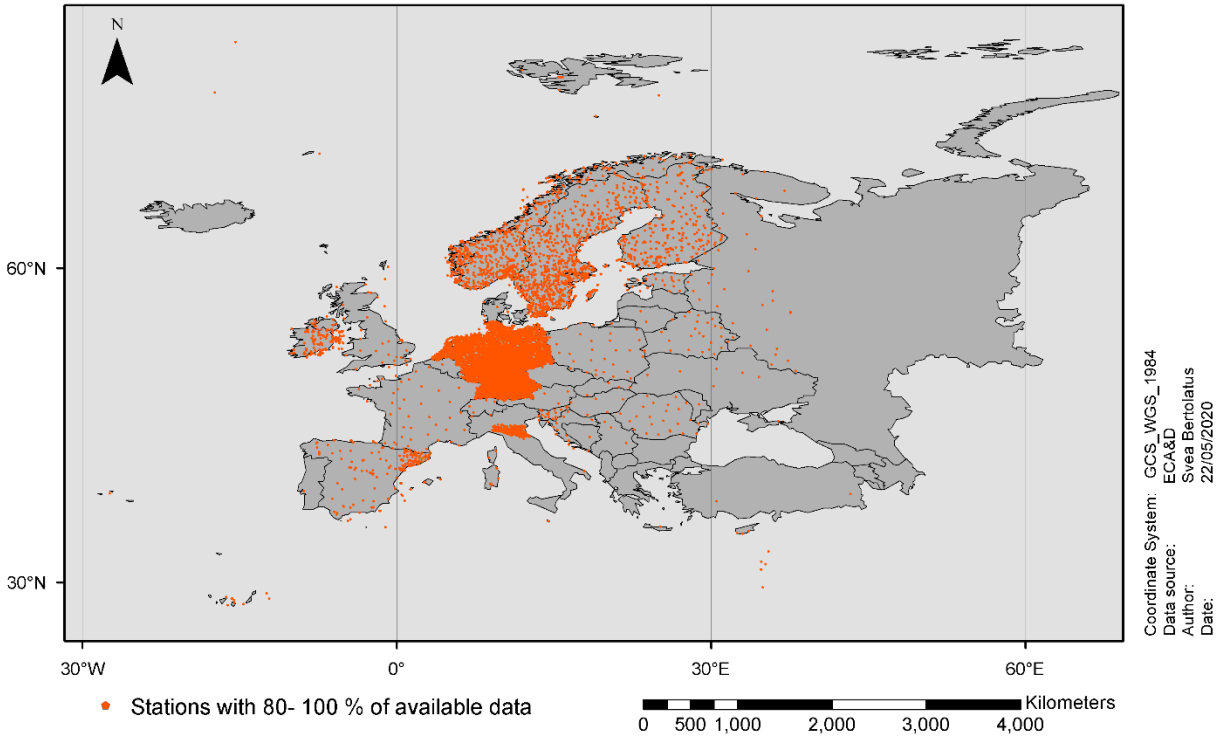

Figure 4: Distribution of ECA&D stations over Europe: Stations with 80 to 100 % of available data, meaning temporal overlap with the GPM data.

3.2.3 Digital Elevation Model (DEM)

The DEM GTOPO30 was clipped to the extent of Europe using ArcMap 10.5. Due to the difference in spatial resolution between DEM and GPM raster cells, several spatial analyst and conversion tools were applied to resample the elevation data into the GPM grid size (0.1°). Thereby the 100 DEM cells, falling into one cell of GPM grid size, were combined by taking the average between them.

3.2.4 Climate Classification

The polygon file of the Köppen climate classification, downloaded from World Bank (World Bank 2017) was edited. The classes were assigned according to a study (Beck et al. 2018), using ArcMap 10.5. The zoom-in locations were within the five largest characterizing climate zones in Europe, and therefore chosen to illustrate potential differences between the characterizing climate zones.

3.3 Data Analysis

The data analysis has been done by using the gauge data group that has >80% of data, which overlaps, temporally seen, with the PMW data, as reference data. The analysis was done by computing error indices, relating results of the Relative Bias to elevation and latitude, and producing time series for locations in different climate classes.

3.3.1 Error Indices

Different error indices have been calculated between each gauge station and its closest satellite grid cell, for each season (Spring: March, April, and May; Summer: June, July, and August; Autumn: September, October, November; and Winter: December, January, and February). The computed error indices are presented in Table 4. In this analysis it was assumed that the ground-based data are the reference dataset for investigating the accuracy of the satellite data.

Root Mean Square Error (RMSE) and the Mean Absolute Error (MAE), measure the average error between the two variables in the unit of the variables. Thus, smaller values of RMSE and also MAE represent a lower error in satellite data comparing with the gauge data. However, there are differences in those two measures: The MAE measures how far the satellite products are averagely away from the ground measurements. The RMSE estimates the square root of the variance of the difference between both variables (residuals) (Grace-Martin 2020). The Relative Bias (Bias) describes the percentage of the error in relative to the absolute value of the reference.

In order to evaluate the ability of the sensors to detect rain events, several more indices were applied. The probability of detection (POD) is thereby a measure of the percentage of correctly detected (by the satellite) rain events out of total observed (by gauge) events. The frequency of hit (FOH) is a measure of how often the rain is detected correctly out of all detections by satellite. In opposite to FOH, the False Alarm Ratio (FAR) estimates the ratio of wrongly classified rain events by the satellite out of all detections by satellite. The critical success index (CSI) assesses the percentage of correctly detected rain events out of the total number of detected or observed rain occurrence.

The Heidke Skill Score (HSS) (Table 2, ID 8) measures the correctly detected proportion for a random forecast.

The outcome of the error indices for each season, distributed over Europe, was visualized using ArcMap 10.5. As cells appeared to be very small in the maps of Europe, zoom in areas were visualized for the Bias to have achieve better visibility of the cell magnitudes. The zoom in was done for the Bias during winter season, as it is an important measure for satellite validations and evaluations.

Table 4: Error indices, for evaluation of the satellite performance relative to gauge measurements over the study area.

ID	Error Indices	Equation	Perfect Value
1	Root Mean Square Error (RMSE) (*in mm/day)*	$RMSE = \sqrt{\frac{\sum_{i=1}^{n}(S_i - G_i)^2}{n}}$	0
2	Mean Absolute Error (MAE) *(in mm/day)*	$MAE = \frac{\sum_{i=1}^{n}\lvert S_i - G_i\rvert}{n}$	0
3	Relative Bias (Bias) *(in %)*	$Bias = \frac{\sum_{i=1}^{n}(S_i - G_i)}{\sum_{i=1}^{n}(G_i)}$	0
4	Probability of Detection (POD)	$POD = \frac{a}{(a+c)} * 100$	100
5	Frequency of Hit (FOH) *(in %)*	$FOH = \frac{a}{a+b} * 100$	100
6	False Alarm Ratio (FAR) *(in %)*	$FAR = \frac{c}{(a+b)} * 100$	0
7	Critical Success Index (CSI) *(in %)*	$CSI = \frac{a}{a+b+c} * 100$	100
8	Heidke Skill Score (HSS) *(in %)*	$HSS = \frac{2(a*d - b*c)}{(a+b)*(b+d)+(a+c)*(c+d)} * 100$	100

Description:

***n* is the total amount of observations/satellite estimates over a certain time period, i.e. number of days; *i* is the *i*th of satellite or gauge data (day *i*); S_i are the satellite estimates at all different location (with matching stations) for day *i*; G_i are the gauge measurements at all different locations for day i; *a* stands for hit (rain event is detected by satellite and observed by station); *b* stands for a false alarm (the rain event was detected but not observed); *c* stands for a missed detection (the rain event was not detected but observed); *d* stands for correctly undetected (the rain event was not detected and not observed).**

3.3.2 Topography

To define a relationship between the error estimates and the topography of Europe, the relative bias was plotted against elevation values and a trend line was displayed. The plots are presented for all seasons in the whole study period (March 2014 to December 2019), where cold seasons has a greater possibility of frozen precipitation, especially in elevated areas.

3.3.3 Climate

Regarding the relationship of the error estimates and climate zones, a local time series for the PMW estimates and gauge measurements were computed for the five introduced locations across Europe (Figure 2), representing the present largest climate zone. This was done in order to receive an insight on how the error in the satellite data differs in different locations and climates of Europe.
The time series was computed over all month during one year, 2015, and presented by classifying it into the different seasons, each presenting three months of daily data in a line plot.

3.3.4 Latitude

The relative bias was plotted against the latitude for all locations having gauge and satellite data, for each season, and for the whole time period. A trend line was added to the scatter plot.

4. Results

4.1 Error Indices

The error indices are presented for each season, covering Europe with all satellite data cells that a station was falling into. Looking at the distribution of the indices, it is referred back to the topography of Europe that was presented in the background section 2.1.1 (Figure 1).

1) Root Mean Square Error:
   Displayed in Figure 5 are the values for the RMSE distributed over Europe and ranging from 0 to over 10 mm/day. Higher values, meaning larger error, are found in southern Germany, northern Italy, and the south-east coast of Norway, in all seasons. Comparing with the DEM (Figure 1), those are areas are of higher elevation.
   Furthermore, seasonal variation in the values are clearly seen: While large parts over Europe, especially Germany, are covered by low RMSE estimates ranging between 0 to 5 mm/day in spring autumn and winter, Large RMSE were found for the summer season . In contrary, the winter season shows large distribution of the lowest RMSE value in eastern Germany, Sweden, and Norway. However, in Norway the values throughout all seasons reach the highest class, compared to the other seasons.

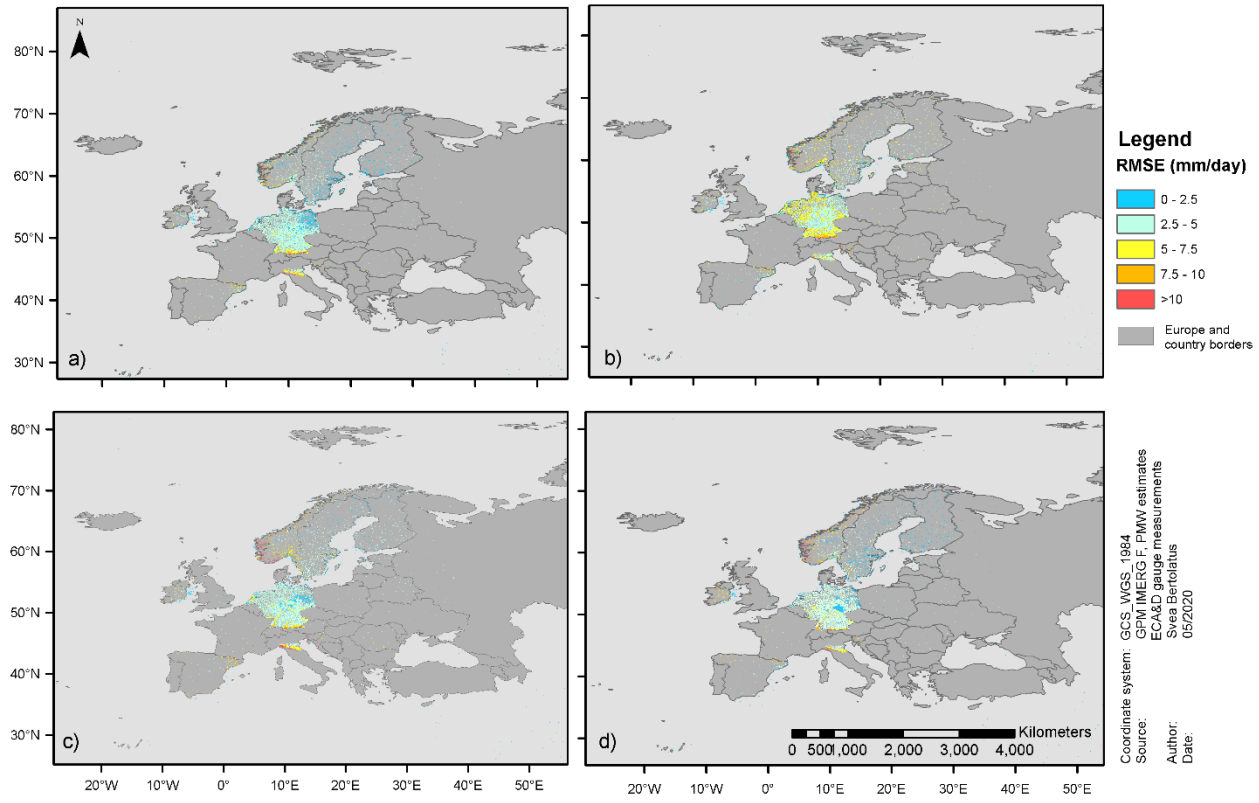

Figure 5: Distribution of Root Mean Square Error (RMSE) between PMW and gauge data over Europe for a) spring, b) summer, c) autumn and d) winter.

2) Mean Absolute Error:

The MAE produces generally lower values for the error estimates, than the RMSE (Figure 6). On the second sight however, it can be seen that elevated areas, such as Alps and the Norwegian mountains show increased values, still below 5 mm/day. . MAE does not show many differences on a large scale over the year, but the error in the Alps is reduced in autumn and winter and the highest in spring (a) and summer (b).

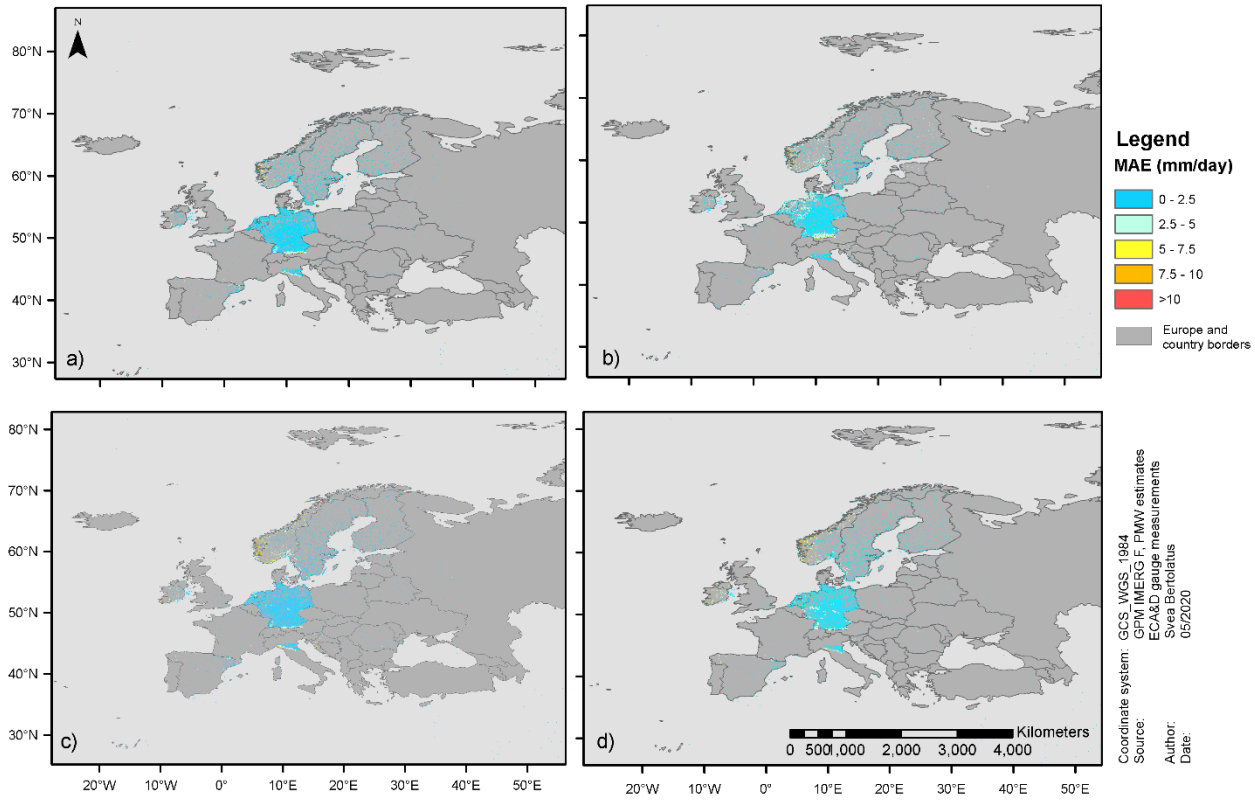

Figure 6: Distribution of Mean Absolute Error (MAE) between PMW and gauge data over Europe for a) spring, b) summer, c) autumn and d) winter.

3) Relative Bias:

Relative bias (Figure 7) with the error direction, are mostly showing negative values over the Europe. The lowest negative values (negative bias) are found in spring, but these values become less negative in summer. In autumn, the values become more negative, and then rise into positive biases or close to 0 in winter. Figure 8 shows a zoom in to certain areas in the winter season: b) Scandinavia, c) eastern Europe, d) Spain and Portugal and e) Germany and northern Italy. High negative Bias can here be seen in for elevated areas in Spain, Northern Italy and Norway.

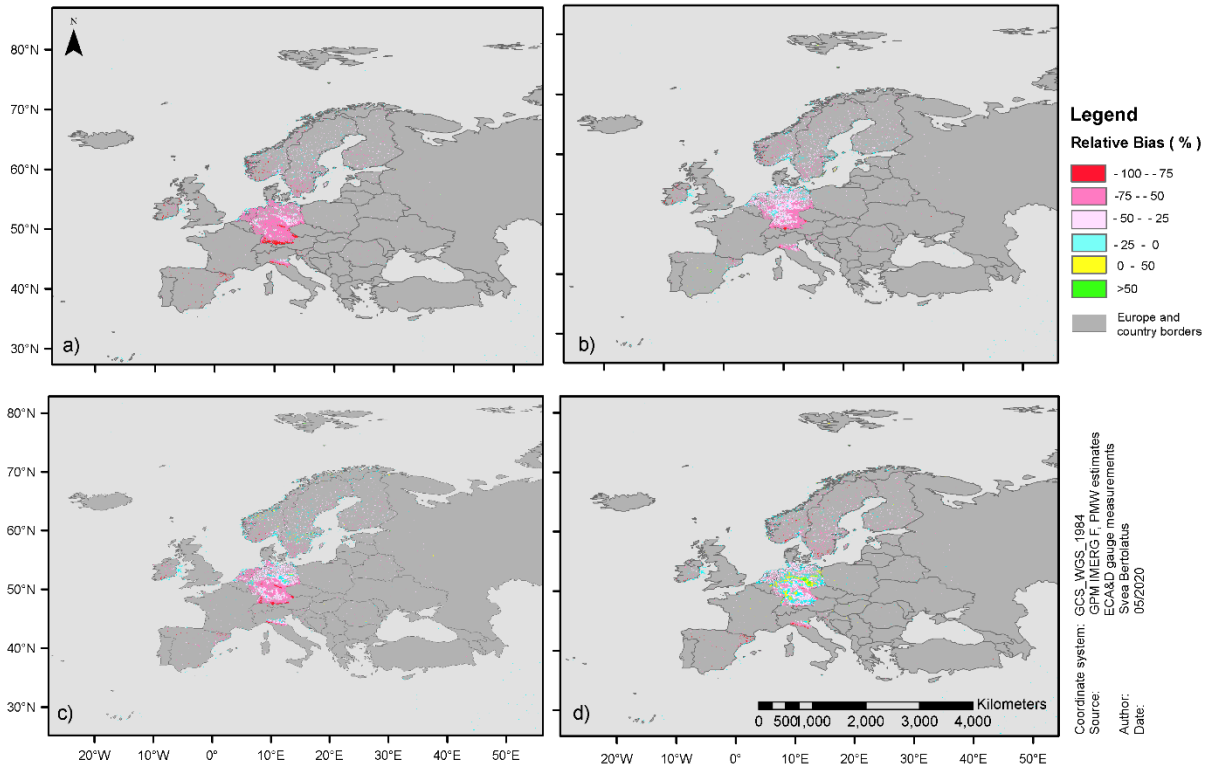

Figure 7: Distribution of Relative Bias (Bias) between PMW and gauge data over Europe for a) spring, b) summer, c) autumn and d) winter

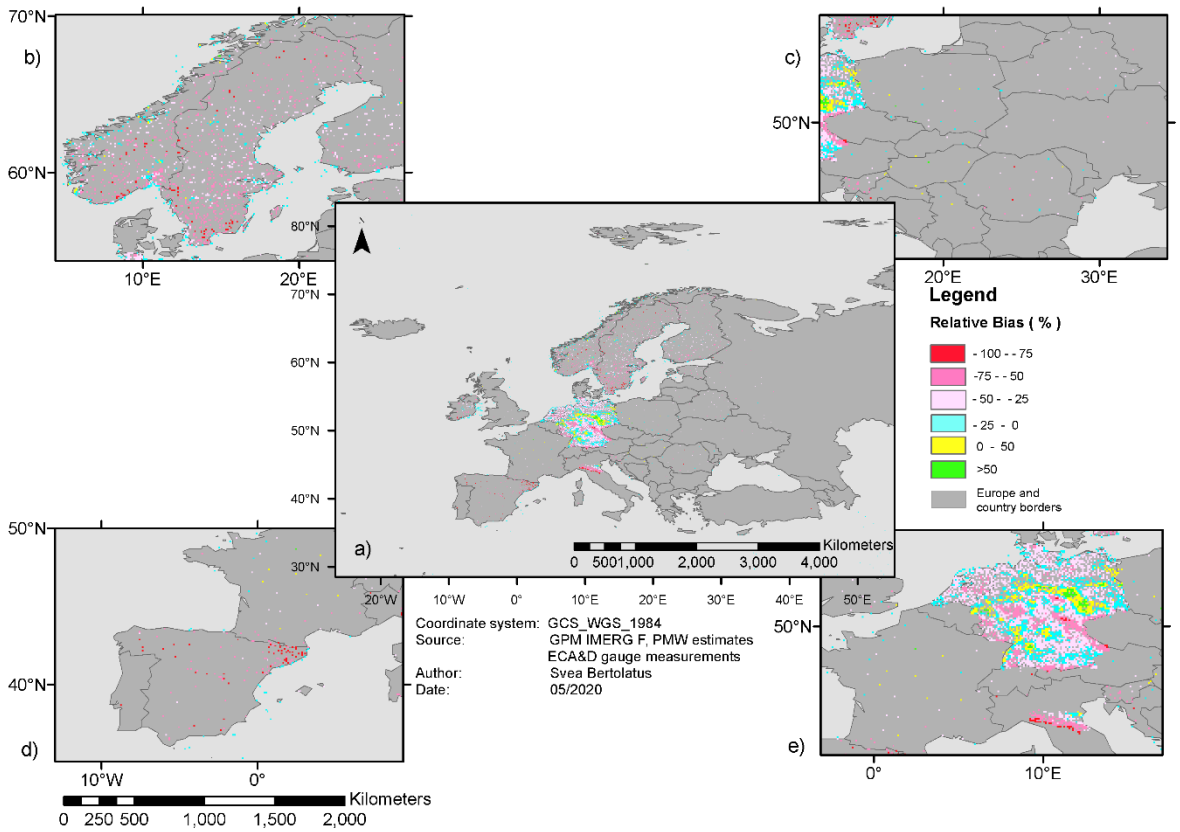

Figure 8: Distribution of Relative Bias (Bias) between PMW and gauge data for winter, a) over Europe, b) Scandinavia, c) eastern Europe, d) Spain and Portugal and e) Germany and northern Italy.

4) Probability of Detection:
The best values of the POD (Figure 9), which is the ratio of correctly detected rain events to total observed events, is 100 %. The assessment over Europe shows the highest (best) values in summer, laying the class of 75 to 100 % in central Europe and 50 to 75 % in Northern East and Southern Europe. The lowest values are shown in spring, where the class of 25- 50 % cover large areas. Europe in autumn and winter is mainly covered by the class of 50 to 75 %. Relations to topography are not visible, despite very low values in Norway in winter can be observed.

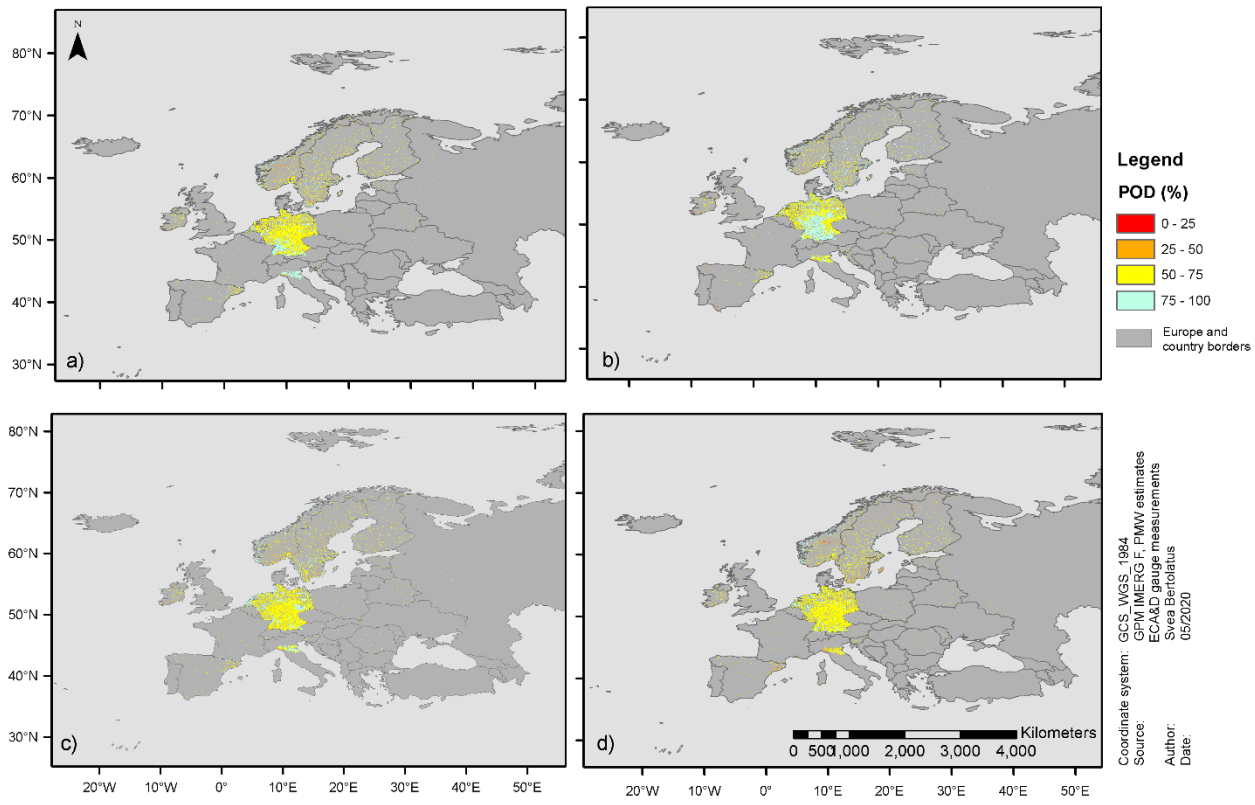

Figure 9: Distribution of Probability of Detection (POD) between PMW and gauge data over Europe for a) spring, b) summer, c) autumn and d) winter.

5) Frequency of Hit:

As for the FOH (Figure 10), the measure of correctly detected rain events out of all detections, the perfect ratio is 100 %. FOH shows gradually increasing values in the cell distribution going from spring to winter, where the highest values are found in winter and the lowest in spring. Spatially seen, values are generally lower in northern Europe and higher in central and southern Europe. Values in northern Italy remain quite low in all seasons.

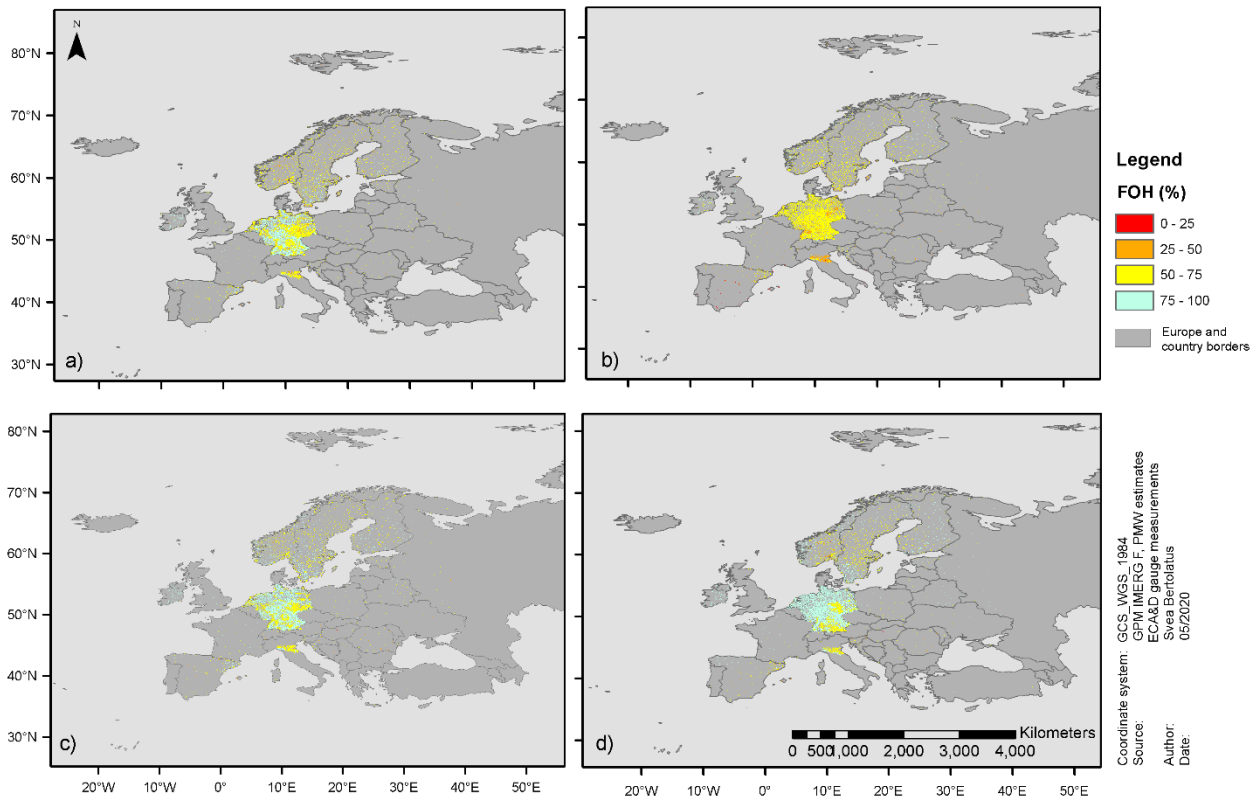

Figure 10: Distribution of Frequency of Hit (FOH) between PMW and gauge data over Europe for a) spring, b) summer, c) autumn and d) winter.

6) False Alarm Ratio:

The FAR (Figure 11), giving the ratio of wrongly detected rain events to all detections by satellite, has the perfect value at 0 %, meaning no false alarm. Values are spatially distributed similar to the FOH estimates, showing the best values in central and southern Europe and a higher percentage for false alarm in northern Europe. Seasonally seen the best values are found in autumn, covering Europe largely with the group of 0- 25 %. Again, the estimates in northern Italy show generally a quite high percentage of false alarms.

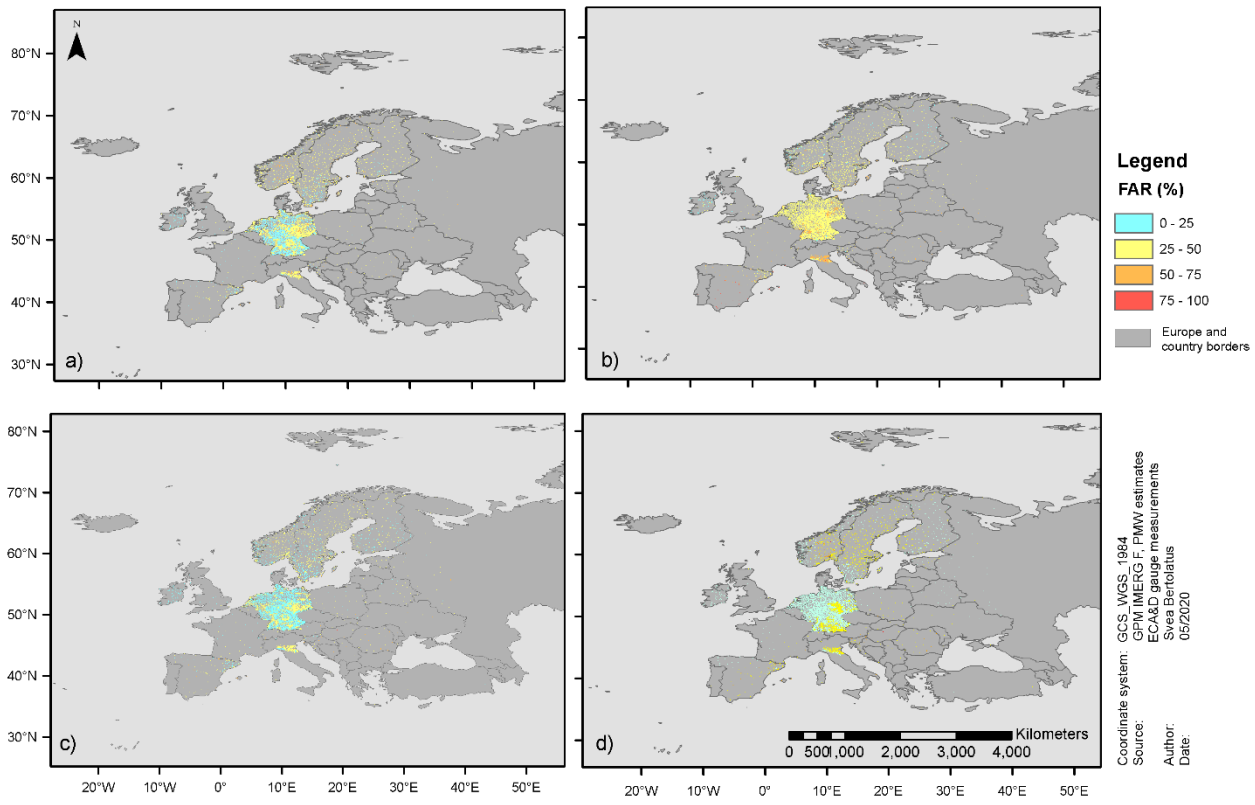

Figure 11: Distribution of False Alarm Ratio (FAR) between PMW and gauge data over Europe for a) spring, b) summer, c) autumn and d) winter.

7) Critical Success Index:
The critical success index (Figure 12), presenting the ratio of correctly detected events out of all observed or detected rain events, with a perfect value of 100 %, performs the worst in spring, having large amounts of cells all over Europe that fall into the lowest possible class, which is 0 to 25%. The value distribution in summer, spring and winter is moderate, values are falling mainly into the class of 50% to 75%. In is visible that values decreasing slightly, also showing in winter are lower in Scandinavia and Northern Italy and Southern Europe than in Central Europe.

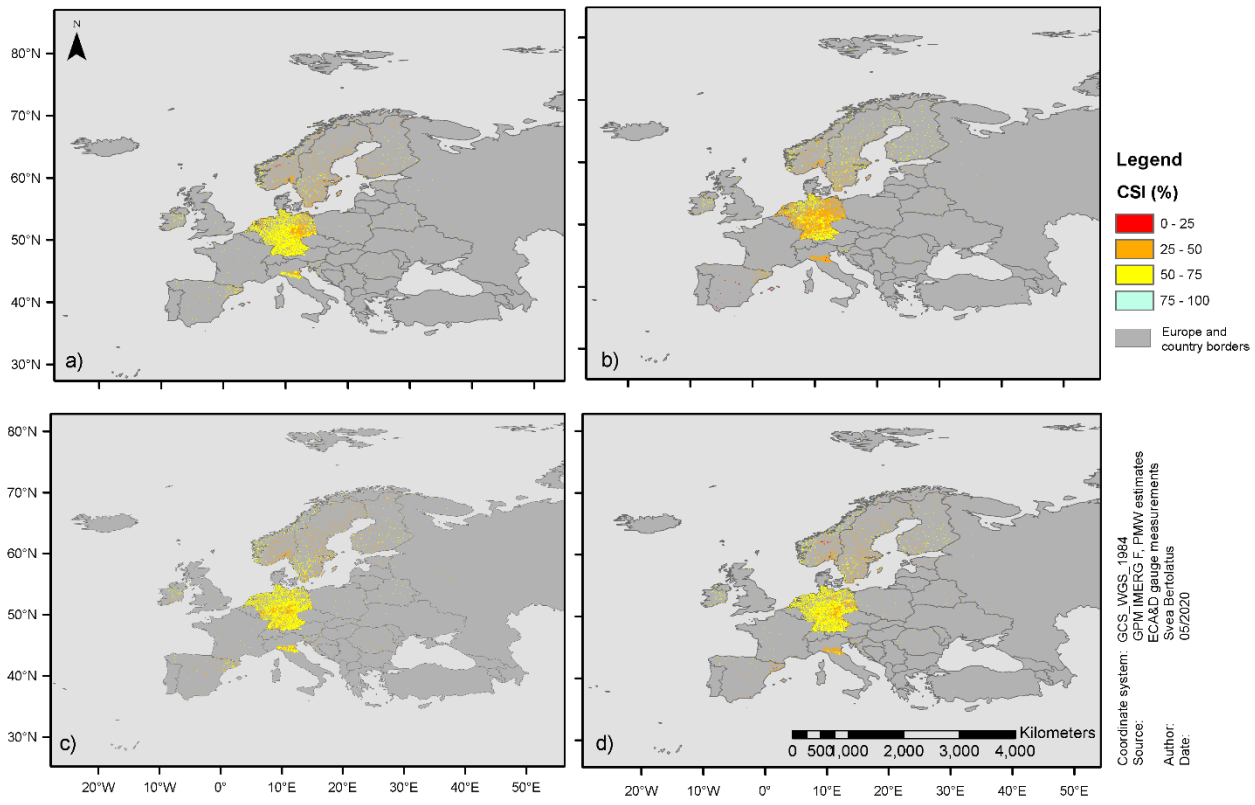

Figure 12: Distribution of Critical Success Index (CSI) between PMW and gauge data over Europe for a) spring, b) summer, c) autumn and d) winter.

8) Heidke Skill Score:

The HSS (Figure 13), assessing the correctly detected proportion in a random forecast, has a perfect value of 100 %. Seasonally seen, summer reaches the highest values, laying largely in the class of 50 to 75 %. Spring is obviously the worst performing season in terms of HSS, where nearly all values are falling into the lowest possible class of 0 to 25 %. Further, the winter season performs low, being dominated by cells showing values of below 50 %. Autumn shows moderate to low values between 0 and 75 %. Over all seasons, it is clearly visible that the values in the North, especially in Norway are very low. Also northern Italy is showing rather low values.

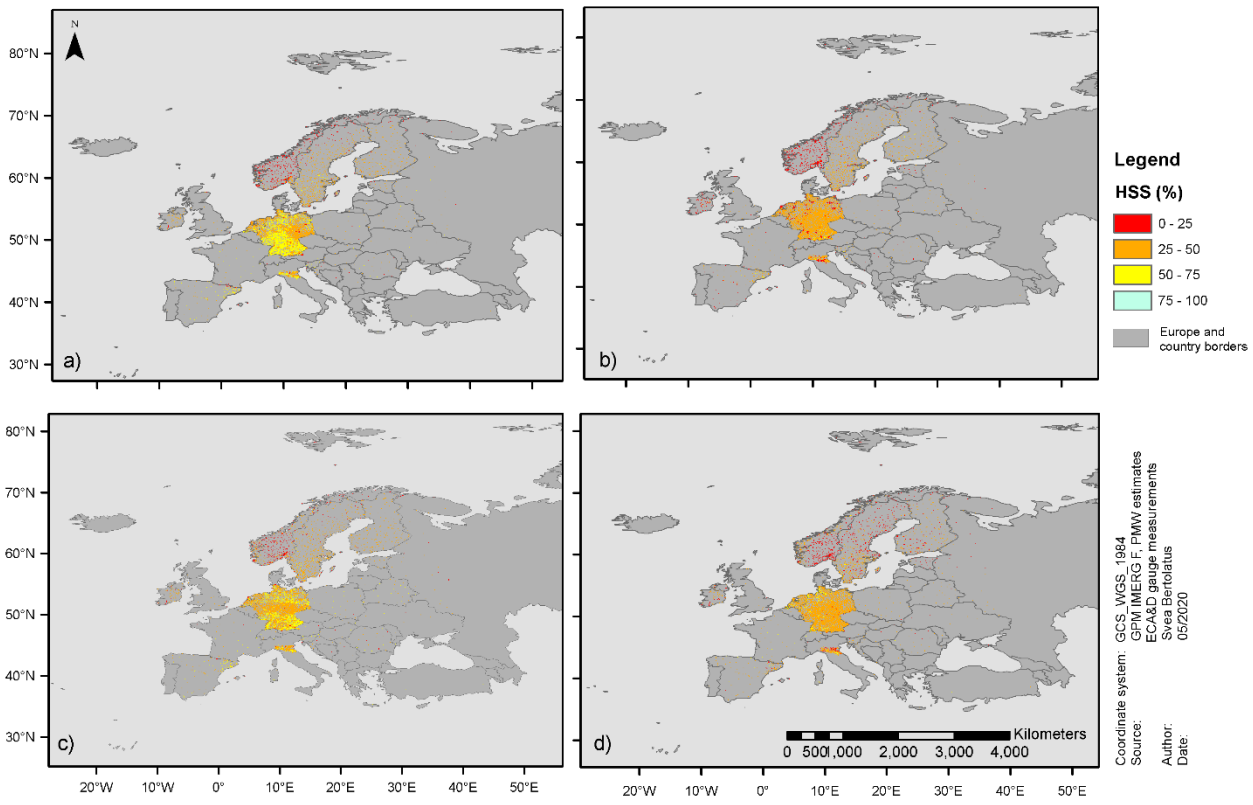

Figure 13: Distribution of Heidke Skill Score (HSS) between PMW and gauge data over Europe for a) spring, b) summer, c) autumn and d) winter.

4.2 Topography

The relation of Relative Bias and elevation is presented for summer and autumn. In both seasons the Relative Bias is scattered mostly below zero meaning that the satellite data underestimates the gauge data. Furthermore, the trend with higher elevations is negative, meaning the trend of the Bias decreases from below 0 towards -100%. As 0 is the perfect value of the Bias, it means that the error estimates between satellite and gauge measurements increases with increasing elevation. Comparing the graphs of summer (Figure 14 b) and winter (Figure 14 d), the Bias seems to be distributed over a broader range in winter, associated with also more bias values are around 0 or a positive bias in low elevations.

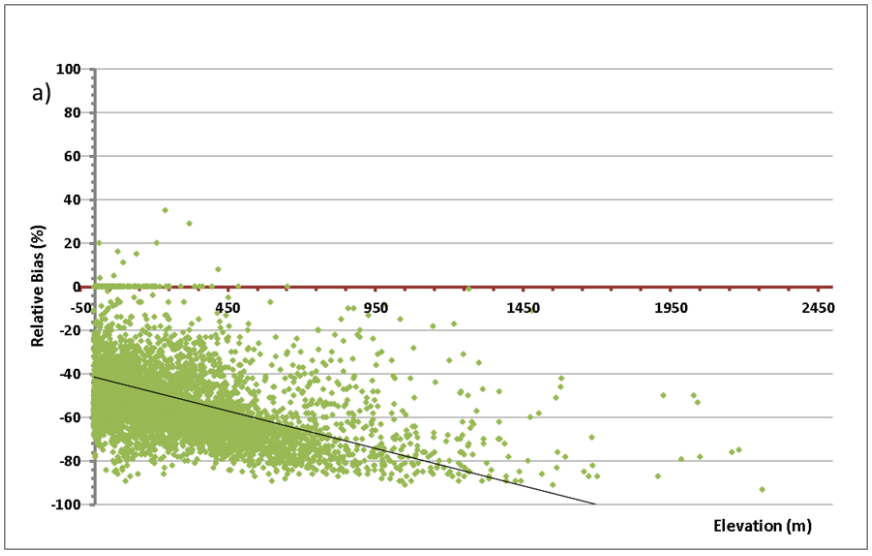

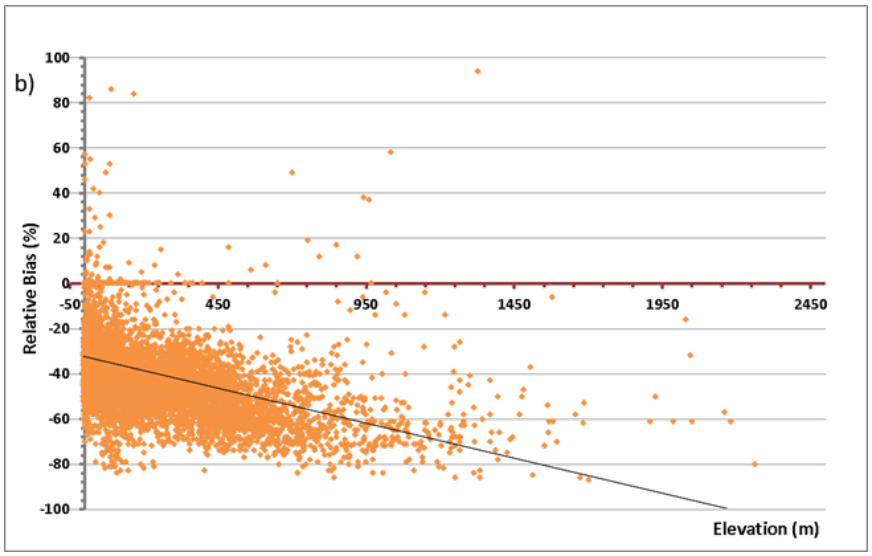

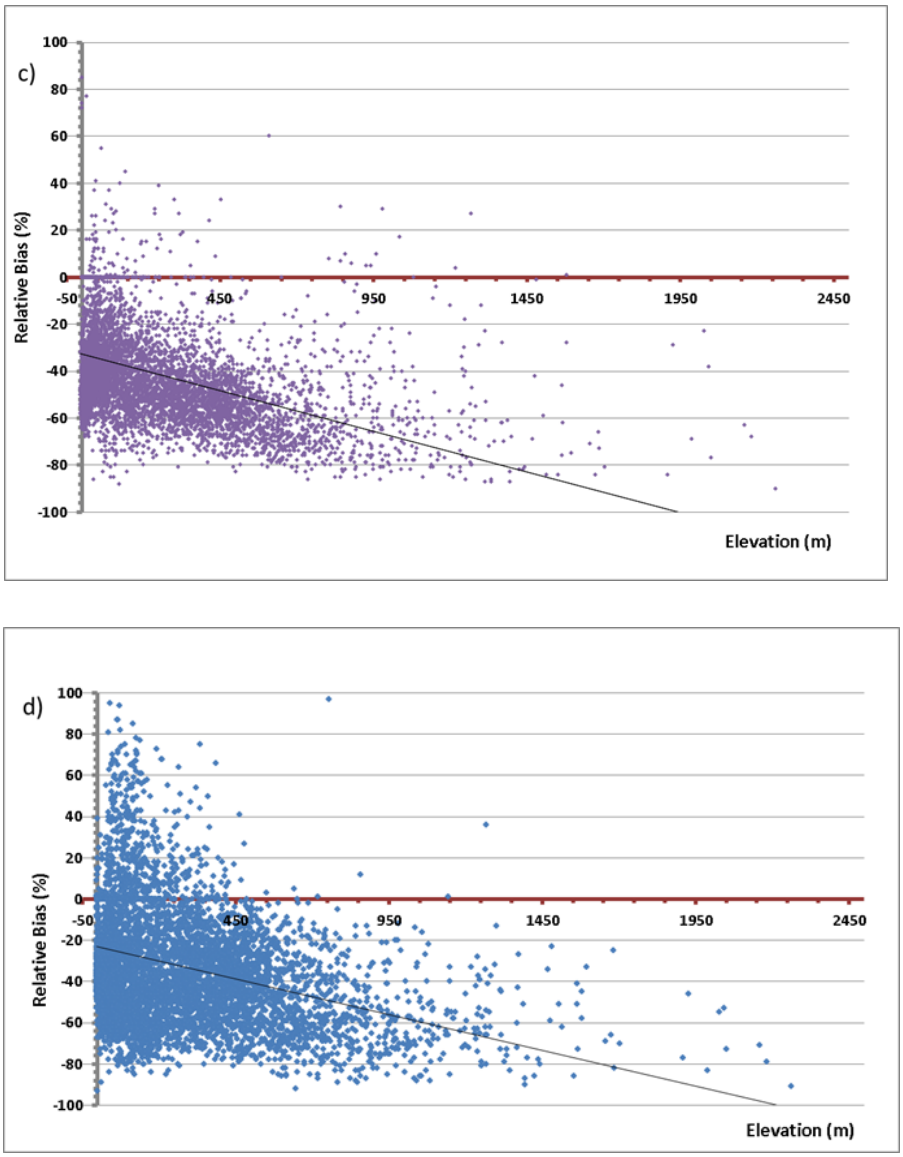

Figure 14: Plot of Relative Bias (%) against Elevation (m) in a) the spring season, b) the summer season, c) autumn season and d) winter season.

4.3 Climate

This section presents the time series of PMW estimates and gauge observations over each day of each season in 2015, for different locations across Europe. Those locations are considered being representative for a climate zone (see 3.1.3). The time series are presented for the locations from highest latitude to lowest latitude.

1) **Svalbard** being located high up in the North, characterized by Tundra climate (ET). The time series of spring and summer (Figure 15) show mainly an over estimation of the PMW estimates compared to the gauge measurements. The highest difference is seen in early spring, March, e.g., in one event the satellite estimate is about 17 mm/day, but the gauge observation is only 5 mm/day.
   Furthermore, in autumn, the rain event estimations and observations of satellite and gauge do not match well, resulting in several overestimations but also underestimations by the satellite.
   The detections agree well again in winter, however the magnitude is being determined by under and over estimations of the PMW product.

Svalbard (78.1500° N, 15.550 ° W)

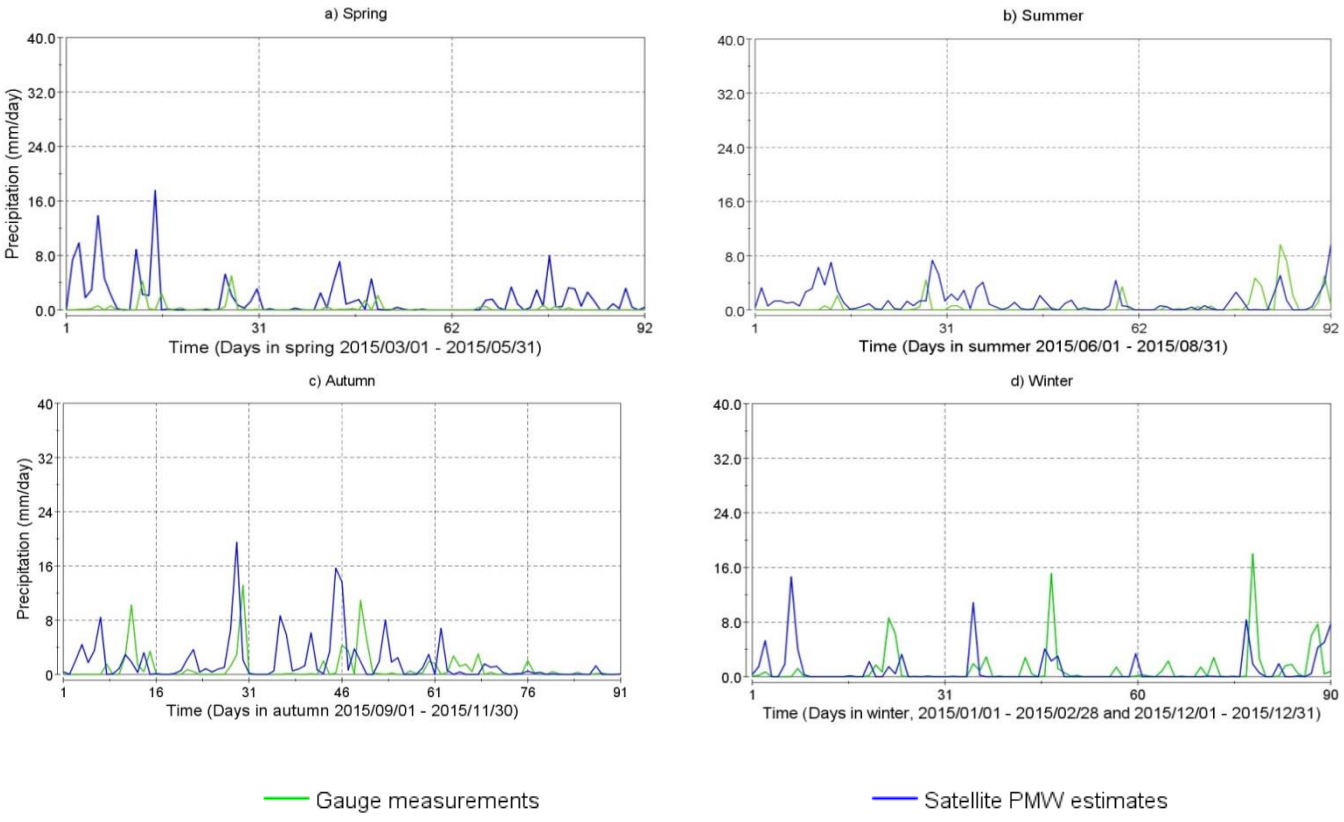

Figure 15: Time series of PMW estimates and gauge measurements for a) spring, b) summer, c) autumn and d) winter in Svalbard.

2) **Oulu** is located in boreal climate (Dfc). The time series show acceptable agreement between PMW estimates and gauge measurements in autumn and winter (Figure 16), with matching rain detections between satellite and gauge and very small differences in magnitude. In spring and summer, the rain detections agree, however, the PMW estimates mostly underestimate the gauge measurements, especially for higher rainfall amount in summer.

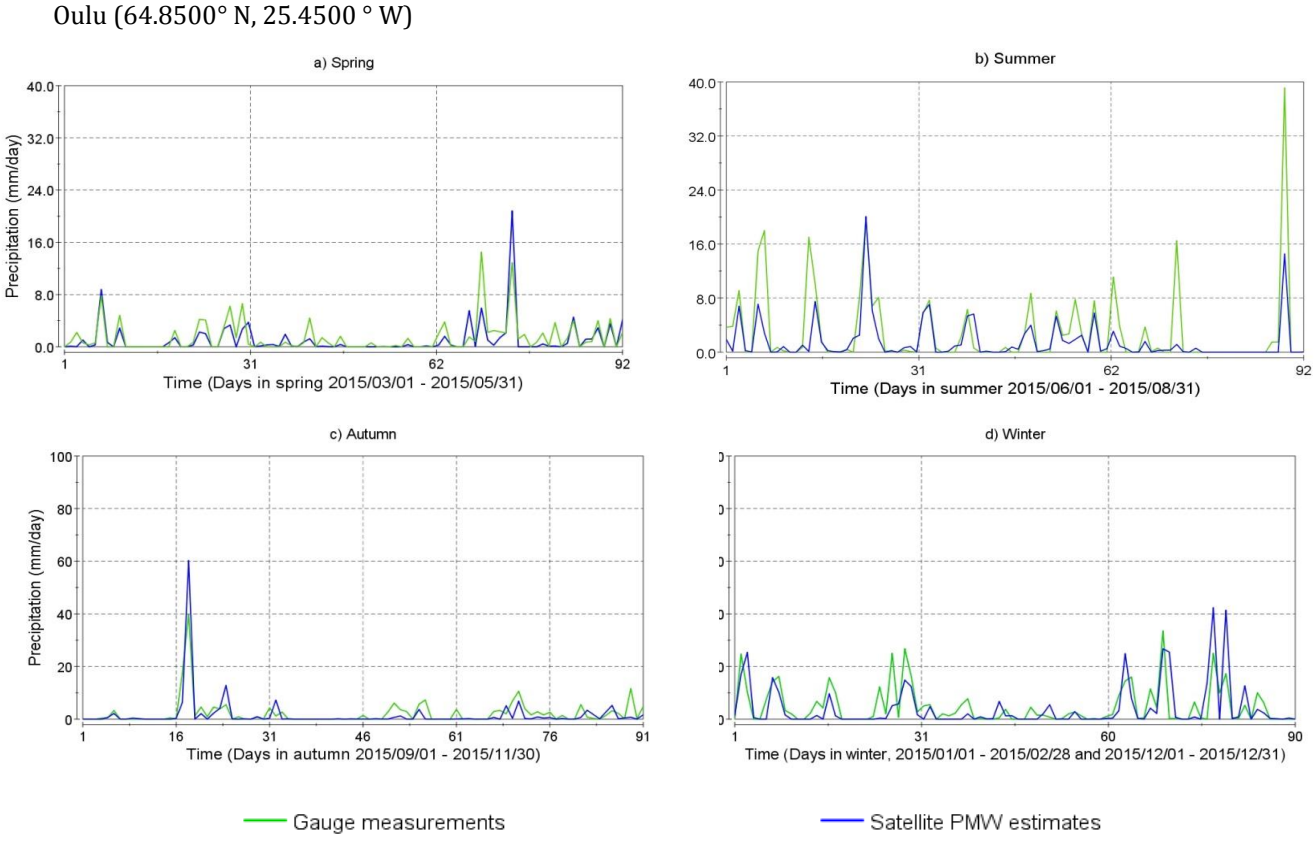

Figure 16: Time series of PMW estimates and gauge measurements for a) spring, b) summer, c) autumn and d) winter in Oulu.

3) **Moscow** located in the warm summer humid continental climate zone (Dfb). The event detection matches moderately between PMW estimates and the gauge observations (Figure 17), counting four detected rain events that were not observed by gauge (three in autumn and one in summer) and six missed rain events, observed by gauge but not by satellite (three in autumn, three in winter). Spring shows just a few rain events, but those are mostly over estimated by the PMW estimates. The other seasons show a consistent underestimation, in summer, where events are characterized by high rainfall, in November (end of autumn) and throughout the winter season.

Moscow (55.65° N, 37.65 ° W)

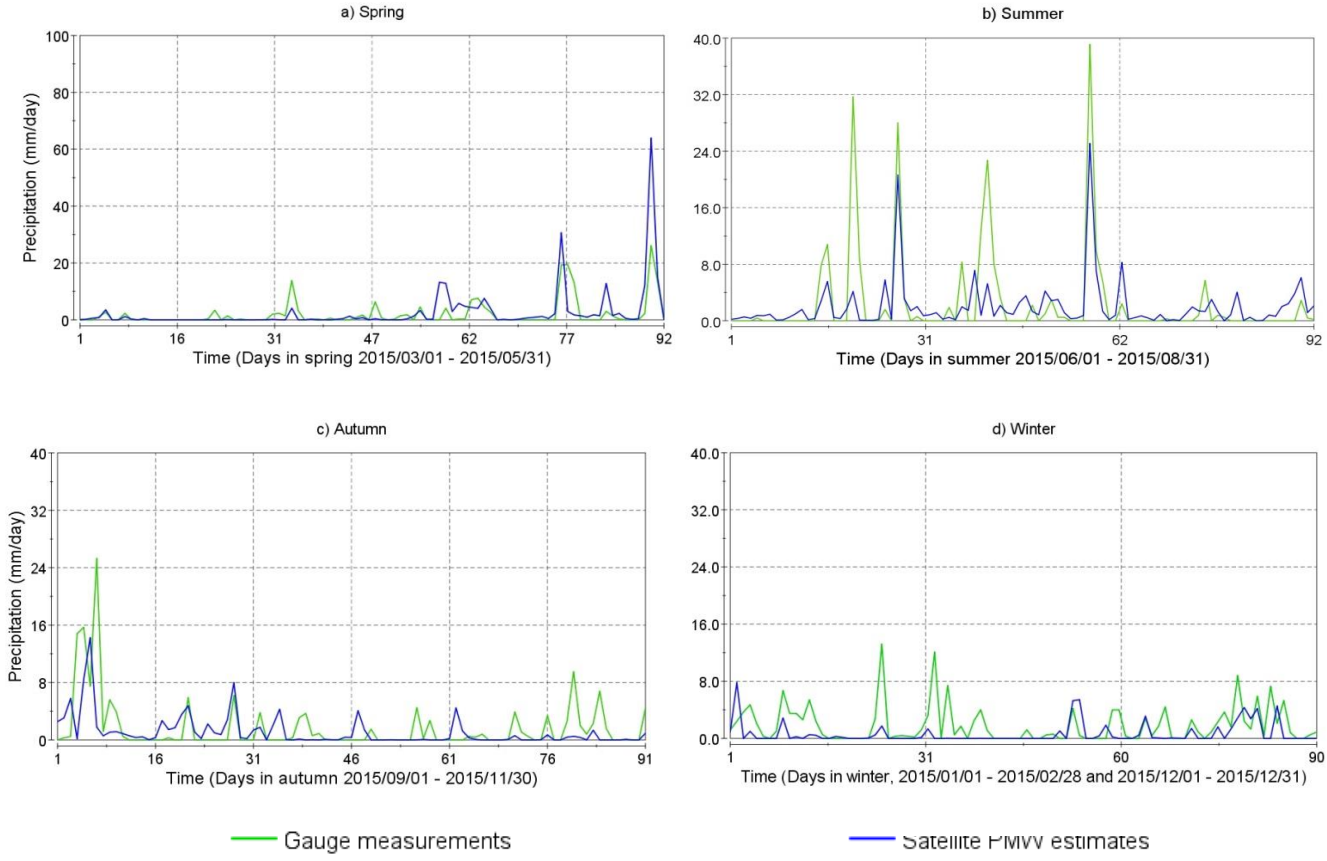

Figure 17: Time series of PMW estimates and gauge measurements for a) spring, b) summer, c) autumn and d) winter in Moscow.

4) **Hamburg** represents a temperate oceanic climate (Cfb), also agrees well in terms of rain event detections/estimation and observations (Figure 18). In terms of magnitude, the satellite and gauge measurements agree well in winter and moderately in autumn and spring, just showing underestimations in November and end of January. However, the summer is characterized by consistent underestimations of the satellite estimates, i.e. out of 14 rain events, 8 are underestimated, and 6 are matching well with the gauge data.

Hamburg (53.550 ° N, 10.050 ° W)

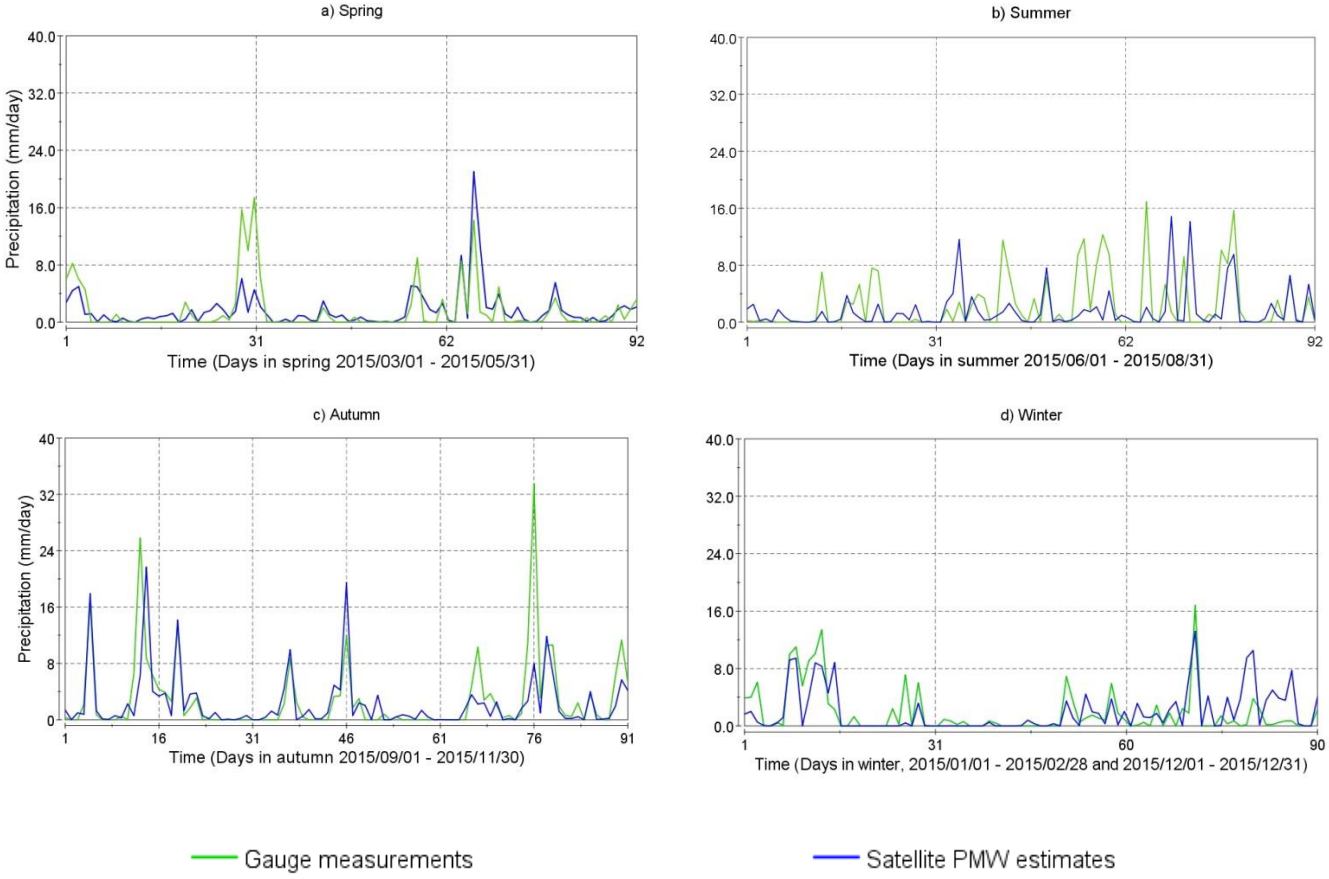

Figure 18: Time series of PMW estimates and gauge measurements for a) spring, b) summer, c) autumn and d) winter in Hamburg.

5) Lastly, **Lisbon** represents the hot-summer Mediterranean climate (Csa). The graphs show less rain (Figure 19), compared to the locations, evaluated earlier. A consistent underestimation by the PMW estimates is noticeable, showing the highest differences to the gauge measurements in autumn, where high rainfall is observed by the gauges. Also, in early December a heavy rain event of above 50 mm/day measured by gauge, is extremely underestimated by the PMW estimates with about 5 mm/day being observed for the same rain event. In autumn and winter there are also many observed rain events, total of nine in those two seasons that were not detected by the satellite. The detection ability is improved in spring and summer, but also here, underestimations are consistent.

Lisbon (38.65° N, -08.75 ° W)

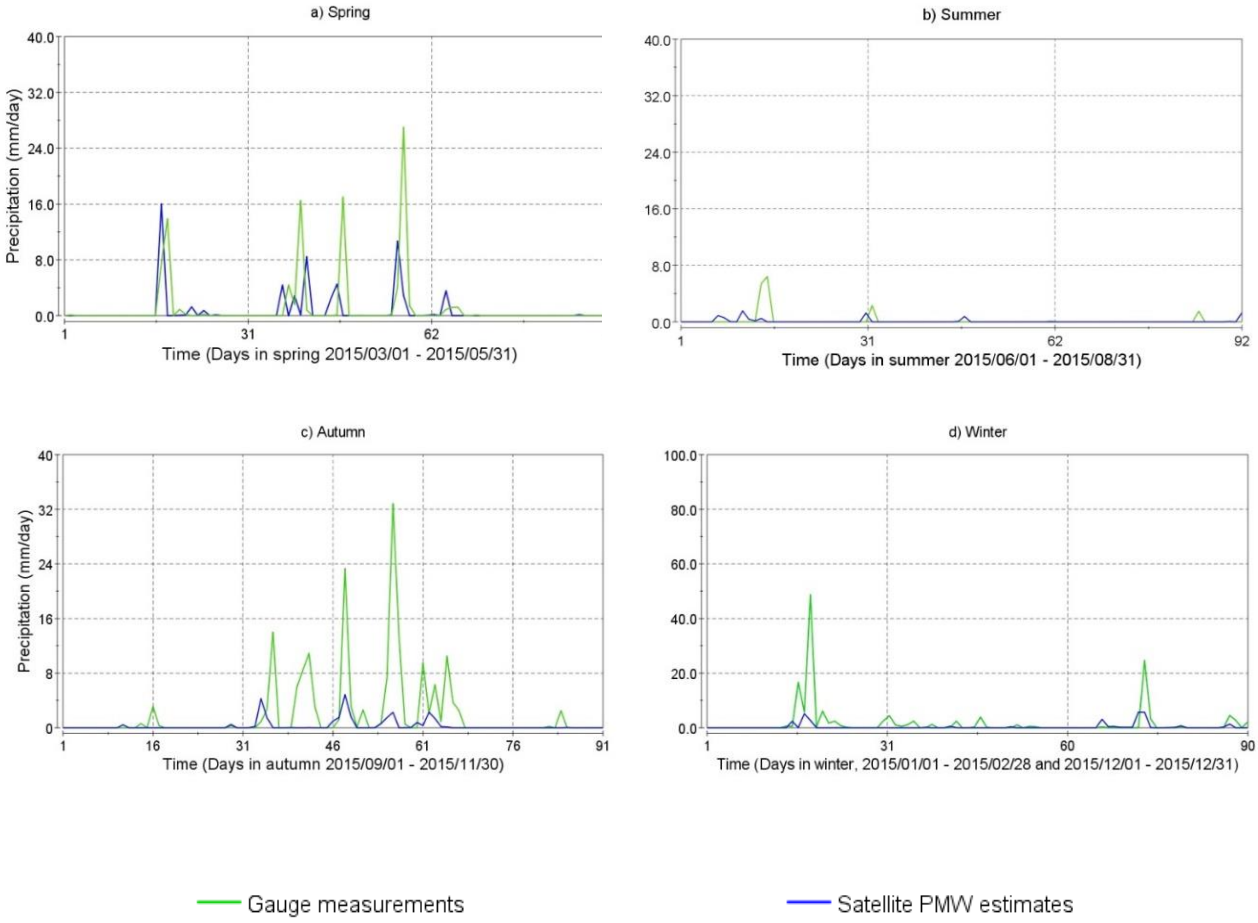

Figure 19: Time series of PMW estimates and gauge measurements for a) spring, b) summer, c) autumn and d) winter in Lisbon.

4.4 Latitude

The Relative Bias is plotted against the latitude (see Figure 20) for summer and winter seasons. As seen in the figure, the relative bias is not changing with latitude for summer, but for winter we observe a negative trend. The perfect value for the Bias would be 0. For spring and autumn a slightly positive trend is seen.

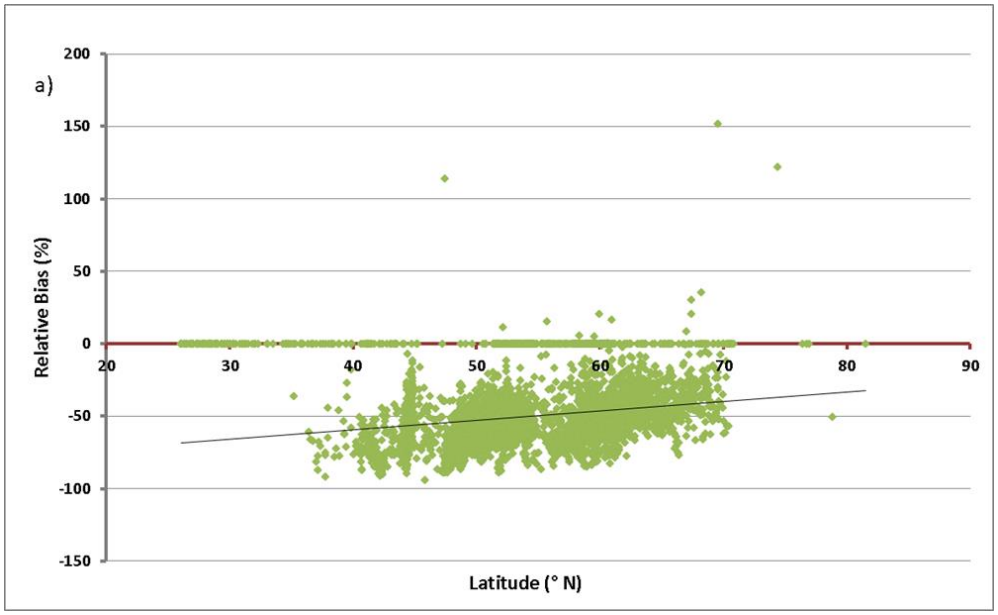

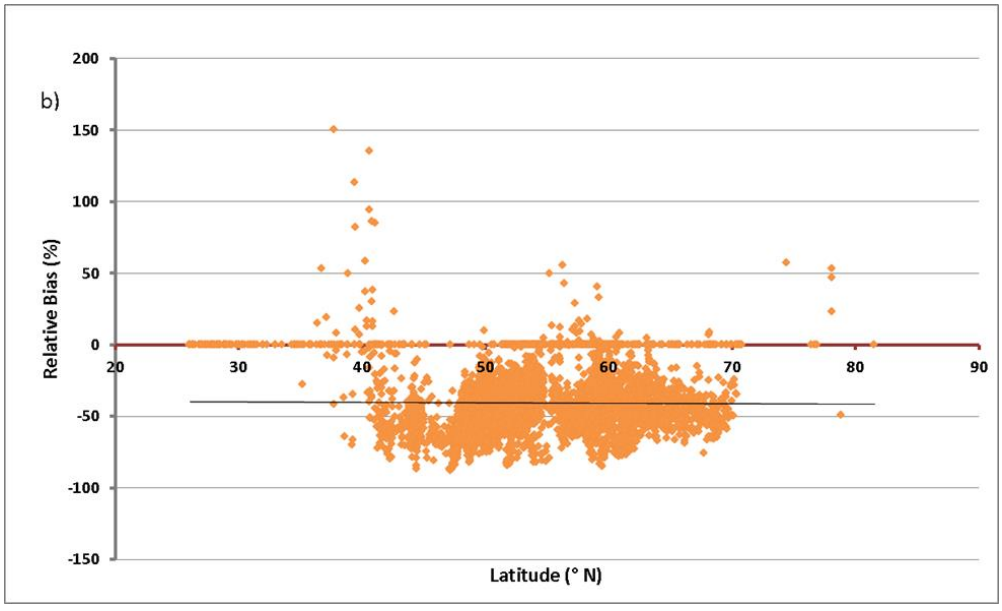

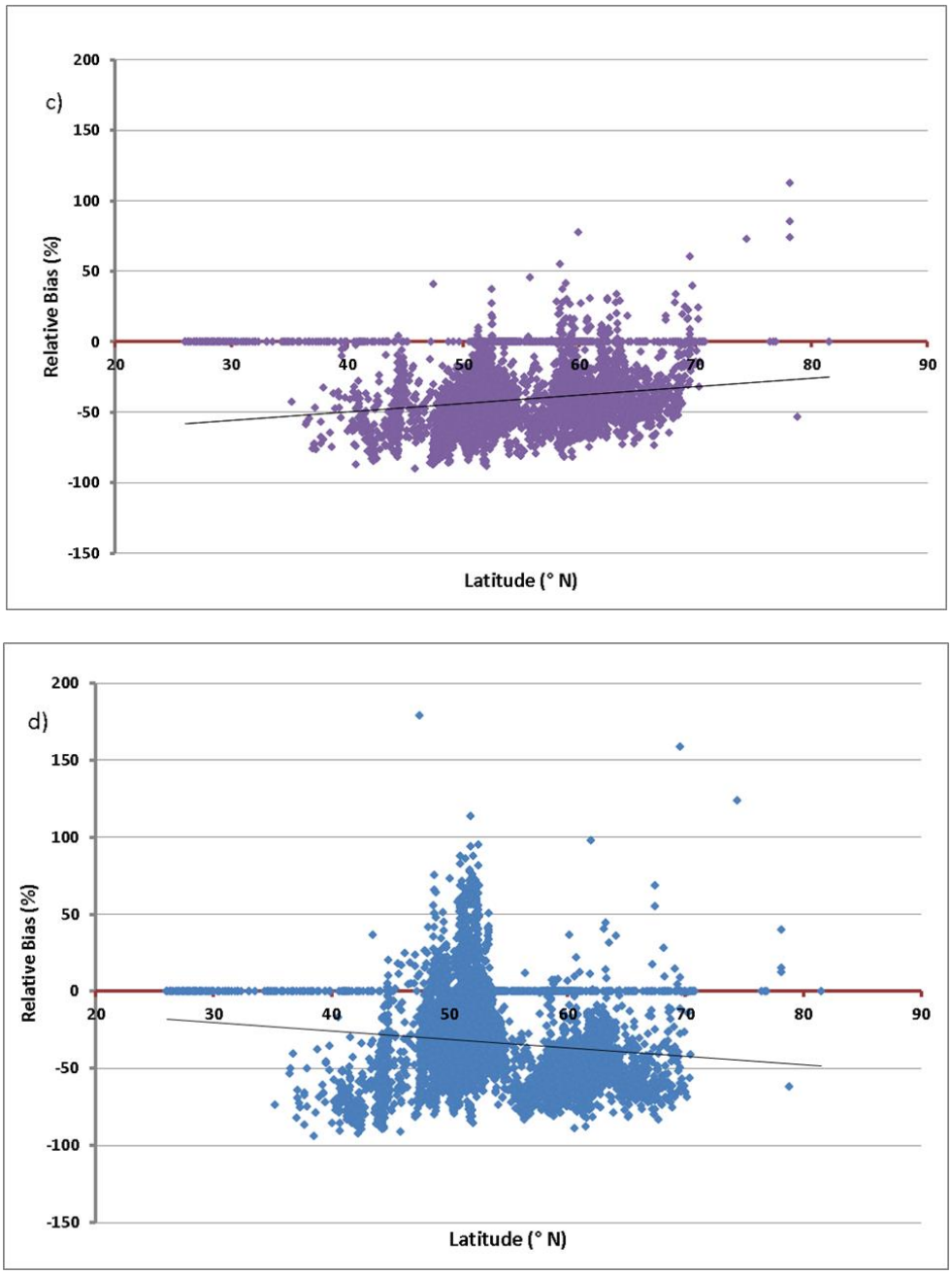

Figure 20: Plot of Relative Bias against latitude in a) the spring season, b) the summer season, c) autumn season and d) winter season.

5. Discussion

This thesis investigated the error characteristics in the PMW data (the main input data to the GPM IMERG product), and its relation to geographical and physical parameters such as elevation, latitude, and climate. The results from this study can be used to identify the sources of possible error in the GPM IMERG products.

5.1 GPM evaluation with gauge data

Different error indices were used to evaluate the difference between the PMW and gauge data. The results showed the performances of PMW data vary between seasons and locations. Seasonally seen, in terms of detection ability, spring showed the worst performance. Probability of detection and Heidke Skill Score showed the best detection ability of PMW in summer. Also, in terms of the difference between the PMW and the gauge measurements the largest bias was obtained for spring. In principle, the better performance of passive microwave measurements in the warm seasons than in the cold ones could be related to the challenges of the PMW sensors for measuring frozen rainfall or from a cold background (Sun et al. 2018). Surprisingly, the spring PMW measurement was less accurate than that of winter for detection ability and measured magnitude relative to gauge measurements. The potential reasons for the low performances in spring could be that the earth's surface is still rather cold after the winter season, causing difficulties to accurately retrieve precipitation by the PMW sensors from a cold background (Sun et al. 2018). However, with this reasoning, the error in winter should be as large as the one in spring. The high error during spring needs to be further investigated.

RMSE showed the worst performance in summer, especially in Germany and further South. In these areas, also FOH and FAR showed slightly better detection ability in autumn and winter, compared to summer. The reason for this can be due to convective systems, which are more common in higher temperature, such as in summer and regions further to the South, leading to bad performances by the satellite observation (Sun et al. 2018). In turn, satellite sensors tend to underestimate precipitation at lower temperature (Wen et al. 2016).
RMSE showed a higher range of values, compared to the other index measuring average error such as MAE. The latter did not show much variation between seasons. This is because, in comparison to MAE, the RMSE gives higher weights to larger errors, resulting in a broader range of values that show the differences. This leads to a higher contrast between values for RMSE, visible already at a small scale (Medium 2016).
By comparing performances in seasons and locations, the PMW measurement for the North, especially Norway, seemed to be less accurate compared to the Central Europe (shown in the maps of RMSE, CSI, and HSS). This can be explained as the area characterized by cold Tundra (ET) and boreal climate (Dfc), potentially causing difficulties measuring with passive microwaves. In cold seasons, PMW measurements are largely influenced by the ice scattering in the atmosphere, and the measurement quality is further reduced, when surfaces covered with snow, as snow causing strong reflection by the covered surface, (Xu et al. 2017).

The underestimations of the satellite measurements in those cold climates were also seen when we checked the time series of precipitation data for the year 2015 in Oulu (a finnish town located in boreal climate) and Svalbard (located in Tundra climate). In Svalbard, the underestimations and missed detections in frequency were mainly present in winter, but with overestimations in other seasons. Svalbard is located at arctic region, and the reason for the worse performance can be linked to the difficulties of satellite sensors in measuring frozen rainfall and also the deviation caused by snow covered surface (NASA 2020). Further, the limited satellite coverage and visibility at high latitudes from the geostationary orbit can also cause some errors in the PMW data (Rødseth 2015). In addition, the strong ionospheric activities close to the poles, meaning a rapid fluctuation in signal amplitude and phase can cause difficulties receiving GPS signals, and thus complicating satellite navigation in high latitude areas (Rødseth 2015; Services 2020). The Arctic Weather Satellite, a planned new satellite initiated as a part of Sweden's Arctic Strategy, (SWS 2020) targets at improving satellite measurements in this Arctic.
For Moscow, located in the humid continental climate zone, PMW also underestimated the precipitation in 2015, especially in the cold season, which is expected. In general, the performance of PMW sensors was better at Moscow comparing with the other two north sites.
Furthermore, the PMW estimates in Hamburg matched quite well with the gauge observations, except for summer. In Hamburg, the warm summer, characterized by convective systems, potentially caused difficulties for satellite sensor's observations and led to generally larger underestimation through the season. These underestimations due to convective systems in a warm climate were also seen in Lisbon throughout the year, located in the hot summer Mediterranean climate zone (Csa). Hence, the strong influence of climate conditions on the satellite PMW accuracy has been illustrated in this study. However, it remains unclear that how far the higher error estimates in the North, seen in the time series, are caused by lacking satellite coverage and how far by a cold climate.

When plotting error estimates (Bias) against latitude, the anticipated loss in accuracy with higher latitude due to the lack of satellite coverage and difficulties sensing light and frozen precipitation in higher latitudes was only observed in winter season. A theory for this can be a better balance of error between low and higher latitudes during summer. Convective systems cause under estimations, resulting in higher error estimates than usual at lower latitudes in Europe. And in the North a better performance should be possible, compared to winter, as the summer is warmer and does not bring the difficulties in cold temperatures for PMW measurements. This can cause the balance of errors in high and lower latitudes in summer that we saw in the constant trend lines in the plot of Relative Bias against latitude in that season, and even lead to a slightly better performance with latitude, as spring and autumn showed.
The relationship between Bias and elevation clearly confirmed the hypothesis of error estimates increasing with elevation, which is shown with the negative trend lines throughout all seasons. The relationship, was shown to be the strongest in winter, having the steepest trend: Warmer temperatures, as they occur in summer, can reduce the error at high elevations, lowering the difficulties for the satellite sensors; and lead to an increase in error estimations at low elevations,

due to convective regimes in a warm temperature. Also, the maps of error indices, showing higher error estimates in elevated areas, support the relationship of the two variables.

Higher positive biases, meaning overestimation by the satellite, was obtained at the coast lines, of e.g., Germany and Norway. These higher positive biases can be caused by sea breeze bringing saturated clouds from the ocean to the coast. Sea breeze often comes in line with weather fronts, resulting in higher precipitation with a high variability in intensity and spatial distribution (Rahmawati and Lubczynski 2018). Especially, when the coastal areas show higher altitudes, as it is the case in Norway, the variability might be even greater. This variability, together with strong wind circulations, makes it difficult for the satellite sensors to quantify the precipitation on the coast. Our results is in agreement with the study of (Rahmawati and Lubczynski 2018) that showed coastal overestimations. Furthermore, the high spatial variability of coastal rains is hard to detect by the satellite, as the spatial resolution of PMW might not be sufficient (each cell covering 0.1° * 0.1°). Furthermore, the common revisit time of the GPM constellation is 3 hours, which could hinder the GPM to capture short-term rain events observed by the gauges at the exact location (Katiraie-Boroujerdy et al. 2013).

5.2 Uncertainties

As already mentioned, spatial and temporal resolution could be a limitation factor in the satellite precipitation estimation for some sites. The grid size of satellite PMW estimates is 0.1° (ca. 11 km^2 on the equator) were compared with the gauges falling into the grid. As the gauge observations are point measurement, hence, they are scaled to be representative for a 0.1°*0.1° area. Depending on weather condition, this mismatch in scales of two datasets cannot be avoided at this regional scale and should be further analyzed in detail, in terms of their impacts on evaluating the satellite performance.

Furthermore, station data vary largely in space. In Central Europe the gauge distribution is very dense, especially Germany and northern Italy, in Northern Europe it is moderately distributed. However, in southern, and eastern parts of Europe as well as islands in the North, such as Iceland, gauges are very sparsely spread. This makes it difficult to visualize results over those areas. The visualization in this study is being enhanced by showing a zoom in to certain areas in the map of the Relative Bias, in order to obtain a better insight on the magnitude of the error distribution, across different areas of Europe.

Around 4000 stations in the ECA&D dataset, having a very small temporal overlap with the GPM period (<20%) 4000, could not be used for the study, resulting in a less dense station distribution for the analysis. Additionally, the reference data can include underestimations as well, especially when the precipitation form is frozen. This might for example explain the satellite overestimates of precipitation accumulation in Svalbard, located in Tundra climate and at high latitude. But also underestimations in both, reference and PMW data, could be possible.

5.3 Further studies

Despite the data limitations, the results from this study showed clear relationships between PMW data accuracy with elevation, latitude, and climate zones in Europe. Evaluation of the PMW data is of paramount importance as it is the crucial data input source to the GPM IMERG products. Correcting those input sources, based on accuracy assessments, such as it was assessed by this study, can be meaningful for further improving IMERG product.

This study can be further improved by a more detailed analysis of the error characteristics by including more locations for time series analysis related to climate influences, and error measures and for different climate zones, separately. It is suggested to compare the outcomes of this study, passive microwave data accuracy, with the combined GPM IMERG products in order to find the relationship between the error in the PMW data with that of the GPM IMERG products. There is also a possibility of developing a correction function to improve the accuracy of the PMW estimates in relation to elevation, latitude, and climate condition.

6. Conclusion

This study evaluated the calibrated PMW estimates (the primary foundation of the GPM IMERG final product) over Europe for the period from March 2014 to the end of December 2019 by using the blended gauge data, provided by European Climate Assessment and Dataset (ECA&D), as reference.

The PMW data was evaluated for each season, by computing different error estimates, comparing the satellite product with the gauge data and linking them to topography, climate and latitude.
The results show clear relationships between PMW data accuracy with elevation and climate zones in Europe that can be linked to difficulties for PMW sensors to measure e.g. frozen precipitation observe from a cold background, or when convection occurs in warmer climates. Regarding the relation to latitude, trends differ between seasons: Winter showed a negative trend towards -100%, that can also be caused by difficulties for PMW sensors to measure e.g. frozen precipitation observe from a cold background at higher latitudes. The other seasons, when frozen precipitation is less likely, however, showed a balanced or even positive trend towards a Bias of 0 (perfect value).
Correcting input sources, like PMW products, based on accuracy assessments, such as it was assessed by this study, can be meaningful for further improvements of the GPM product.

References

Conservation Biology Institute (CBI). 2010. 30 arc-second DEM of Europe (Data Basin Dataset). https://www.arcgis.com/home/item.html?id=e01c7a4f13e9455d880427c1daa19110: ArcGIS.

National Aeronautics and Space Administration (NASA). 2014. Global Precipitation Measurement. https://gpm.nasa.gov/precipitation-measurement-missions: NASA.

National Aeronautics and Space Administration (NASA). 2020. GCPEx Measuring Frozen Precipitation.

B, V., and C. Singh. 2015. Evaluation of error in TRMM 3B42V7 precipitation estimates over the Himalayan region. *Journal of Geophysical Research: Atmospheres,* 120**:** n/a-n/a. DOI: 10.1002/2015JD023779

Bank, T. W. 2017. World Maps Of The Köppen-Geiger Climate Classification. https://datacatalog.worldbank.org/dataset/world-maps-k%C3%B6ppen-geiger-climate-classification: The world bank.

Beck, H. E., N. E. Zimmermann, T. R. McVicar, N. Vergopolan, A. Berg, and E. F. Wood. 2018. Present and future Köppen-Geiger climate classification maps at 1-km resolution. *Scientific data,* 5**:** 180214-180214. DOI: 10.1038/sdata.2018.214

Dataset, E. C. A. 1998. https://www.ecad.eu/: EDA&D.

Fadia, M. F., H. Hashemi, S. H. Hosseini, and R. Berndtsson. 2020. Ground Validation of GPM IMERG Precipitation Products over Iran In *Remote Sensing*.

Gebregiorgis, A., P.-E. Kirstetter, Y. Hong, J. Gourley, G. Huffman, W. Petersen, X. Xue, and M. Schwaller. 2018. To what extent is the Day-1 GPM IMERG satellite precipitation estimate improved as compared to TRMM TMPA-RT? *Journal of Geophysical Research: Atmospheres*. DOI: 10.1002/2017JD027606

Geographic, N. 1996. Europe: Physical Geography. Retrieved 29.04.2020, from http://education.nationalgeographic.com/encyclopedia/europe-physical-geography/

Hashemi, H., J. Fayne, R. Knight, and V. Lakshmi. 2017. *High-resolution Monthly Satellite Precipitation Product over the Conterminous United States*.

Huffman, G.J., E.F. Stocker, D.T. Bolvin, E.J. Nelkin, J. Tan. 2019. *GPM IMERG Final Precipitation L3 1 day 0.1 degree x 0.1 degree V06*. Edited by Andrey Savtchenko. Greenbelt, Maryland. Goddard Earth Sciences Data and Information Services Center (GES DISC). Retrieved 01.04.2020, from 10.5067/GPM/IMERGDF/DAY/06

Hirpa, F. A., M. Gebremichael, and T. Hopson. 2009. Evaluation of High-Resolution Satellite Precipitation Products over Very Complex Terrain in Ethiopia. *Journal of Applied Meteorology and Climatology,* 49**:** 1044-1051. DOI: 10.1175/2009JAMC2298.1

Katiraie-Boroujerdy, P.-S., N. Nasrollahi, K.-l. Hsu, and S. Sorooshian. 2013. Evaluation of satellite-based precipitation estimation over Iran. *Journal of Arid Environments,* 97**:** 205-219. DOI: https://doi.org/10.1016/j.jaridenv.2013.05.013

Lee, J., E.-H. Lee, and K.-H. Seol. 2019. Validation of Integrated MultisatellitE Retrievals for GPM (IMERG) by using gauge-based analysis products of daily precipitation over East Asia. *Theoretical and Applied Climatology,* 137**:** 2497-2512. DOI: 10.1007/s00704-018-2749-1

Maggioni, V., E. I. Nikolopoulos, E. N. Anagnostou, and M. Borga. 2017. Modeling Satellite Precipitation Errors Over Mountainous Terrain: The Influence of Gauge Density, Seasonality, and Temporal Resolution. *IEEE Transactions on Geoscience and Remote Sensing,* 55**:** 4130-4140. DOI: 10.1109/TGRS.2017.2688998

Mindat.org, H. I. o. M. 2000. The Köppen Climate Classification. https://www.mindat.org/climate-Cfb.html: Mindat.org.

Navarro, O. García, Merino, Sánchez, Kummerow, and Tapiador. 2019. Assessment of IMERG Precipitation Estimates over Europe. *Remote Sensing,* 11**:** 2470. DOI: 10.3390/rs11212470

Nazemi, A., M. Alam, and A. Elshorbagy. 2014. Uncertainties in future projections of extreme rainfall at fine scales: The role of various sources.

Network, E. M. S. EUMETNET. About us Retrieved 05.05.2020, from https://www.eumetnet.eu/about-us/.

Rahmawati, N., and M. W. Lubczynski. 2018. Validation of satellite daily rainfall estimates in complex terrain of Bali Island, Indonesia. *Theoretical and Applied Climatology,* 134**:** 513-532. DOI: 10.1007/s00704-017-2290-7

Resources, S. E. O. 2000. TRMM. Retrieved 20.04.2020, from https://earth.esa.int/web/eoportal/satellite-missions/t/trmm.

Rødseth, Ø. J. 2015. Measured Performance of Satellite Systems

in the Arctic. Retrieved, from https://thedigitalship.com/conferences/presentations/2015bergen/day2/DSBergen2015_Ornulf_Jan_Rodseth_Research_Director_Marintek.pdf.

Services, S. W. 2020. About Ionospheric Scintillation. Retrieved 26.05 2020, from https://www.sws.bom.gov.au/Satellite/6/3.

Silva Lelis, L. C., R. W. Duarte Bosquilia, and S. N. Duarte. 2018. Assessment of Precipitation Data Generated by GPM and TRMM Satellites. *Revista Brasileira de Meteorologia,* 33**:** 153-163.

Sun, Q., C. Miao, Q. Duan, H. Ashouri, S. Sorooshian, and K.-L. Hsu. 2018. A Review of Global Precipitation Data Sets: Data Sources, Estimation, and Intercomparisons. *Reviews of Geophysics,* 56**:** 79-107. DOI: 10.1002/2017RG000574

Sunilkumar, K., A. Yatagai, and M. Masuda. 2019. Preliminary Evaluation of GPM-IMERG Rainfall Estimates Over Three Distinct Climate Zones With APHRODITE. *Earth and Space Science,* 6**:** 1321-1335. DOI: 10.1029/2018EA000503

Tan, J., G. Huffman, D. Bolvin, and E. Nelkin, 2020. IMERG V06 Ground Validation Wishlist. National Aeronautics and Space Administration (NASA), Report, https://gpm.nasa.gov/sites/default/files/document_files/IMERG-Validation-Wishlist.pdf. [in Swedish, English summary]

Tang, L., Y. Tian, and X. Lin. 2014. Validation of Precipitation Retrievals over Land from Satellite-based Passive Microwave Sensors. *Journal of Geophysical Research: Atmospheres,* 119. DOI: 10.1002/2013JD020933

Wen, Y., A. Behrangi, B. Lambrigtsen, and P.-E. Kirstetter. 2016. Evaluation and Uncertainty Estimation of the Latest Radar and Satellite Snowfall Products Using SNOTEL Measurements over Mountainous Regions in Western United States. *Remote Sensing,* 8**:** 904. DOI: 10.3390/rs8110904

World., H. i. a. M. 2016. MAE and RMSE — Which Metric is Better? Retrieved 20.05. 2020, from https://medium.com/human-in-a-machine-world/mae-and-rmse-which-metric-is-better-e60ac3bde13d.

Xu, R., F. Tian, L. Yang, H. Hu, H. Lu, and A. Hou. 2017. Ground validation of GPM IMERG and TRMM 3B42V7 rainfall products over southern TibFetan Plateau based on a high-density rain gauge network. *Journal of Geophysical Research: Atmospheres,* 122**:** 910-924. DOI: 10.1002/2016JD025418

Zhang, Y., Y. Ren, G. Ren, and G. Wang. 2019. Bias Correction of Gauge Data and its Effect on Precipitation Climatology over Mainland China. *Journal of Applied Meteorology and Climatology,* 58**:** 2177-2196. DOI: 10.1175/jamc-d-19-0049.1